Bioactive Materials 29 (2023) 132–150

Contents lists available at ScienceDirect

Bioactive Materials

journal homepage: www.keaipublishing.com/en/journals/bioactive-materials

An injectable conductive hydrogel with dual responsive release of rosmarinic acid improves cardiac function and promotes repair after myocardial infarction

Linghong Zhang [a], Zhongwu Bei [a], Tao Li [b], Zhiyong Qian [a,*]

[a] Department of Biotherapy, Cancer Center and State Key Laboratory of Biotherapy, West China Hospital, Sichuan University, Chengdu, 610041, China
[b] Department of Pediatric Cardiac Surgery, West China the Second Hospital, Sichuan University, Chengdu, 610041, China

ARTICLE INFO

Keywords:
Myocardial infarction
Responsive hydrogel
Rosmarinic acid
Conductivity
Combined treatment

ABSTRACT

Myocardial infarction (MI) causes irreversible damage to the heart muscle, seriously threatening the lives of patients. Injectable hydrogels have attracted extensive attention in the treatment of MI. By promoting the coupling of mechanical and electrical signals between cardiomyocytes, combined with synergistic therapeutic strategies targeting the pathological processes of inflammation, proliferation, and fibrotic remodeling after MI, it is expected to improve the therapeutic effect. In this study, a pH/ROS dual-responsive injectable hydrogel was developed by modifying xanthan gum and gelatin with reversible imine bond and boronic ester bond double crosslinking. By encapsulating polydopamine-rosmarinic acid nanoparticles to achieve on-demand drug release in response to the microenvironment of MI, thereby exerting anti-inflammatory, anti-apoptotic, and anti-fibrosis effects. By adding conductive composites to improve the conductivity and mechanical strength of the hydrogel, restore electrical signal transmission in the infarct area, promote synchronous contraction of cardiomyocytes, avoid induced arrhythmias, and induce angiogenesis. Furthermore, the multifunctional hydrogel promoted the expression of cardiac-specific markers to restore cardiac function after MI. The in vivo and in vitro results demonstrate the effectiveness of this synergistic comprehensive treatment strategy in MI treatment, showing great application potential to promote the repair of infarcted hearts.

1. Introduction

Cardiovascular disease is the disease with the highest human mortality rate in the world, causing more than 17.9 million deaths each year, accounting for more than 40% of deaths. Its mortality rate is higher than that of various cancers, and it has brought a heavy burden to the global society and economy [1,2]. Myocardial infarction (MI) is caused by interruption of blood supply, inducing necrosis or apoptosis of cardiomyocytes [3]. After MI, the extracellular matrix (ECM) continues to degrade, resulting in scarring, thinning of the ventricular wall, and ventricular dilatation [4], ultimately leading to heart failure [5,6]. Cardiomyocytes are terminally differentiated and the heart has limited capacity for regeneration. The common clinical treatments for MI include drug therapy, percutaneous coronary intervention, and heart transplantation. However, drug therapy and interventional therapy can only delay the process of ventricular remodeling, but cannot restore the infarcted myocardium [7]. Heart transplantation is limited by insufficient donor organ sources and immune rejection. Therefore, new and improved therapeutic strategies are urgently needed to improve the therapeutic effect of MI.

Tissue engineering and regenerative medicine appear to be promising solutions for myocardial repair after MI [8,9]. Among them, hydrogels with excellent biocompatibility, porous internal structure, tunable mechanical strength, and ability to mimic the ECM in tissues have been widely studied in the treatment of post-MI. Hydrogels can not only provide an ECM-like microenvironment for damaged cardiomyocytes, but also provide mechanical support for the weakened ventricular wall [10–12]. Intramyocardial injection of hydrogel combined with bioactive substances can effectively improve cardiac function after MI and inhibit left ventricular (LV) remodeling [13–17]. For example, alginate hydrogel loaded with melanin nanoparticles can eliminate reactive oxygen species (ROS) to resist oxidative stress

Peer review under responsibility of KeAi Communications Co., Ltd.
* Corresponding author.
E-mail address: anderson-qian@163.com (Z. Qian).

https://doi.org/10.1016/j.bioactmat.2023.07.007
Received 11 May 2023; Received in revised form 5 July 2023; Accepted 5 July 2023
Available online 12 July 2023

damage in cardiomyocytes [17]. In addition, compared with traditional therapeutic agent-loaded hydrogels, the smart-responsive hydrogels can achieve precise on-demand therapeutic agent release at the lesion site, enhance local pharmacological effects, and reduce dosing frequency and side effects of drugs [18,19]. For example, the complex formed by microRNA-21-5p and mesoporous silica nanoparticles (MSNs) was loaded into the hydrogel formed by polyethylene glycol and cyclodextrin to achieve controlled on-demand microRNA-21-5p delivery triggered by a locally acidic microenvironment. The released MSN complex significantly suppressed the inflammatory response and promoted local neovascularization by inhibiting the polarization of M1 macrophages in the infarcted myocardium [20].

Pathological development after MI can be divided into three distinct but overlapping phases, namely inflammation, proliferation, and fibrotic remodeling [13]. Within hours of ischemia, cardiomyocytes die in large numbers, and apoptotic cardiomyocytes release ROS and other cellular contents into the niche to trigger inflammation [21,22]. The proliferative phase is capillary sprouting and fibroblast ingrowth to form granulation tissue, with initial deposition of collagen fibers and continued inflammatory infiltration [23]. The fibrotic stage in which granulation tissue is replaced by dense collagen forms a non-conductive fibrotic scar, resulting in abnormal electrical transmission in the heart [24]. Although a large number of injectable hydrogels have been designed for research on the treatment of MI, most hydrogel systems often lack electrical conductivity, and their therapeutic effects only target a single stage of the pathological development of MI. Therefore, designing a multifunctional conductive drug-loaded hydrogel to meet the needs of different stages after MI may lead to better therapeutic effects.

Rosmarinic acid (RA), an active ingredient presents in a variety of plants including rosemary, is one of the most important polyphenolic antioxidants. In previous disease treatment studies, RA has exhibited biological activities such as anti-inflammation [25], inhibition of apoptosis [26] and anti-fibrosis [27], showing a strong cardioprotective effect. However, its therapeutic efficacy is hampered by its high instability, poor water solubility, difficulty in passing biological barriers, and poor bioavailability [28]. Polydopamine (PDA) is formed by the oxidative polymerization of dopamine, and the catechol active groups on its surface can adsorb a large number of drug molecules [29]. PDA can load a large amount of RA through hydrogen bond interaction and electrostatic adsorption, and realize the slow release of RA.

Research has shown that the conductive hydrogel can restore electrical signaling in scar tissue and promote synchronized contraction of viable heart muscle tissue [30,31]. Polypyrrole (PPy) has the characteristics of easy processing, adjustable conductivity, and good conductivity and electrical stability under ambient conditions, which makes it an attractive conductive polymer. However, practical applications are limited due to its water insolubility and mechanical fragility [32,33]. Previous studies have demonstrated that grafting PPy onto biocompatible gelatin improves its water solubility while endowing the hydrogel with excellent electrical conductivity [34].

Therefore, in this study, combining the hydrogel conductivity with the cardioprotective effects of RA such as anti-inflammation, anti-apoptosis, and anti-fibrosis, a pH and ROS dual-responsive hydrogel was designed for different stages of the pathological development of MI. As shown in Scheme 1, oxidized xanthan gum grafted with 3-aminophenylboronic acid (OXP) has a large number of aldehyde groups and phenylboronic acid groups, and gelatin and dopamine grafted gelatin (GD) have a large amount of amino and catechol groups. A double-network self-healing hydrogel was constructed through the Schiff base reaction between amino groups and aldehyde groups combined with the boronate reaction between phenylboronic acid and catechol. RA was

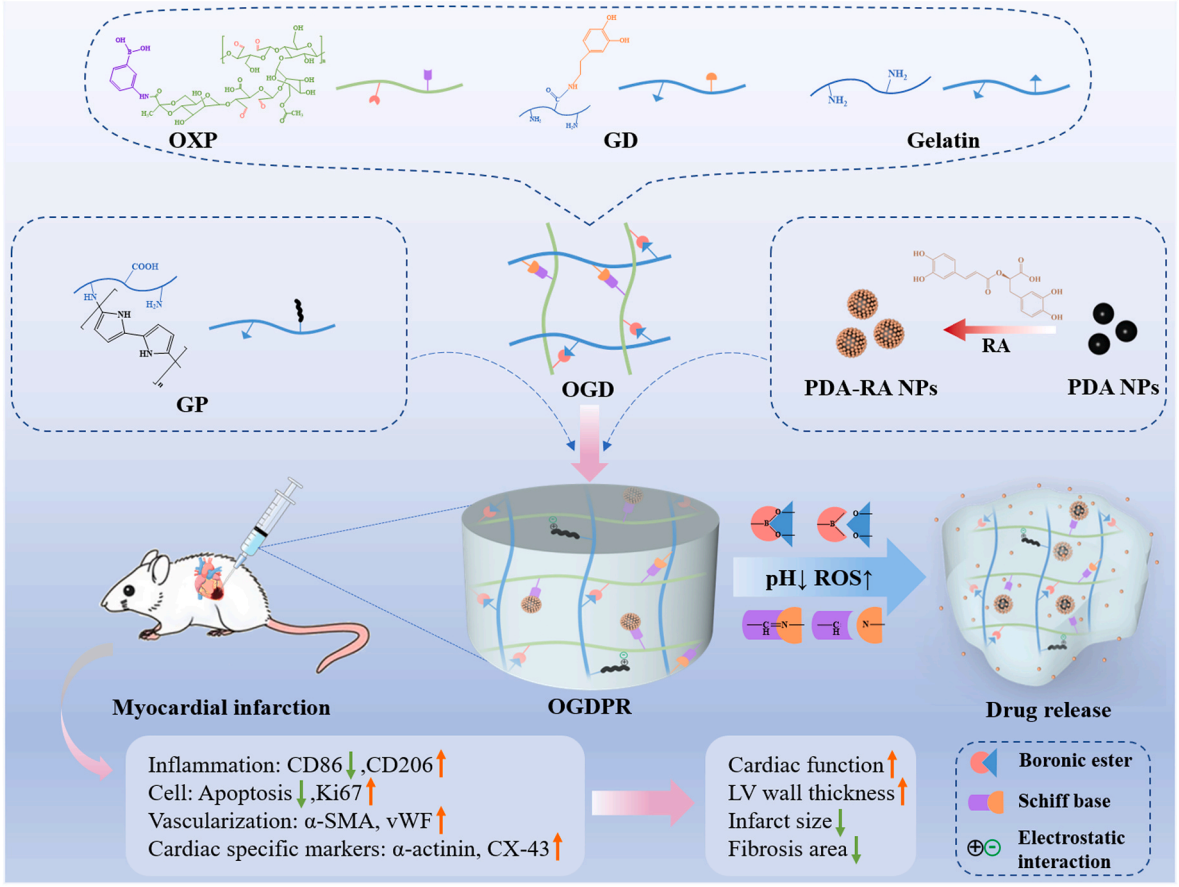

Scheme 1. Schematic illustration of the preparation of a pH/ROS dual-responsive conductive hydrogel encapsulating PDA-RA NPs and its use in MI treatment.

adsorbed on the surface of PDA through hydrogen bonding and electrostatic interaction to form drug-loaded PDA-RA nanoparticles (PDA-RA NPs), which were further loaded into the hydrogel. Nanoparticles can be immobilized in hydrogels by forming boronic ester bonds between catechol groups and phenylboronic acid groups. Adding the highly water-soluble conductive complex PPy-modified gelatin (GP) into the hydrogel network increases the conductivity of the hydrogel while improving the mechanical strength of the polymer network through electrostatic interaction and Schiff base reaction. The boronic ester bond can be broken in response to the high ROS and slightly acidic environment in the MI microenvironment, thereby releasing the drug on demand. We expect that this composite hydrogel can rapidly release RA to inhibit inflammation, regulate macrophage phenotype, improve MI microenvironment, and reduce cell apoptosis in the early stage of MI. In the long term, it can continuously inhibit fibrosis formation, promote angiogenesis and maintain electrical signal transmission in the infarct area. Combined with the mechanical support of the hydrogel, this strategy is expected to improve the overall therapeutic effect.

2. Materials and methods

2.1. Materials

Gelatin (medium gel strength) was purchased from Sigma-Aldrich. Xanthan gum (XG, USP), rosmarinic acid (RA, 97%), 3-aminophenylboronic acid (PBA, ≥98%), dopamine hydrochloride (98%), ferric chloride ($FeCl_3$, AR, 98%), sodium periodate ($NaIO_4$, AR, 99.8%), 1-ethyl-3-(3-dimethylaminopropyl)-carbodiimide (EDC, >98%) and N-hydroxysuccinimide (NHS, AR) were purchased from Aladdin Industrial Inc. Pyrrole was provided by Kefeng Industrial (China). 2, 2-Biphenyl-1-picrylhydrazyl (DPPH, >97%) was purchased from Shanghai Macklin Biochemical Technology Co., Ltd. CCK-8 was purchased From Shanghai Topscience Biotechnology Co., Ltd. Live/dead cell staining kit were purchased from KeyGen Biotech (China). Dulbecco's modified Eagle's medium (DMEM), penicillin/streptomycin, and fetal bovine serum (FBS) were purchased from Gibco (USA). Matrigel was purchased from Corning (USA).

2.2. Preparation and characterization of PDA-RA NPs

Mix 40 mL of ethanol with 90 mL of deionized water and 2.5 mL of ammonia (28%–30%) at 30 °C for 0.5 h. Dissolve 500 mg of dopamine powder in 10 mL of deionized water, and then add the above mixed solution. After 24 h, the precipitate was separated by centrifugation at 12,000 rpm, and then washed three times with deionized water to obtain PDA NPs. Dissolve 8 mg PDA in 10 mL deionized water, add RA in different mass ratios, adjust the pH to 2.5 with 1 M hydrochloric acid, stir for 4 h at room temperature in the dark, and centrifuge to collect the precipitate to obtain PDA-RA NPs. The concentration of RA in the supernatant was measured by a UV–Vis spectrophotometer according to a standard curve, the drug loading and encapsulation efficiency were calculated, and the UV spectra of RA, PDA and PDA-RA were measured. The particle size and zeta potential of the PDA and PDA-RA were measured with a particle size analyzer (ZEN3590, Malvern, UK), and the average values of three tests were recorded. The morphology of nanoparticles was observed and recorded by transmission electron microscopy (TEM).

2.3. Preparation and characterization of the hydrogels

To obtain OGD hydrogels, PBS solutions of OXP, gelatin, and GD were prepared, and the three were mixed to achieve final concentrations of 0.75 wt%, 2.3 wt%, and 0.2 wt%, respectively. GP was added to the above mixed solution at a final concentration of 3 wt%, and OGDP hydrogel was formed after thorough mixing. PDA-RA NPs was added to OGD and OGDP gel systems according to the final concentration gradient of 0.05–1.6 wt% to prepare OGDR and OGDPR hydrogels, and the infrared spectra of all hydrogels were recorded. The gelation time of the hydrogels was studied by using the "inverted bottle method" at 37 °C. The cross-sectional morphology of the hydrogel was obtained by scanning electron microscopy (SEM; JSM-7500F, JEOL, Japan).

2.4. Equilibrium swelling test of hydrogels

The swelling capacity of the hydrogels was determined gravimetrically. The initially dried samples were weighed, and the mass was recorded as W_0, and subsequently immersed in 0.01 M PBS at 37 °C for swelling. At predetermined time points, the hydrogels were removed from the PBS, the surface of the hydrogels were gently wiped with filter paper to remove excess water, and then weighed (W_t). The swelling ratio of different hydrogels was calculated by the following formula:

$$\text{Swelling ratio}\ (g/g) = (W_t - W_0)/W_0$$

where W_0 and W_t are the initial weight and the weight of hydrogel at time t, respectively.

2.5. In vitro drug release study of hydrogels

In order to investigate the release behavior of RA, 100 μL of OGDR and OGDPR hydrogels were prepared in centrifuge tubes. Add 3 mL of PBS solution (pH = 7.4), PBS solution (pH = 7.4) containing H_2O_2 (200 μM), PBS solution (pH = 5.0), and PBS solution (pH = 5.0) containing H_2O_2 (200 μM) to the tube, respectively, and incubated at 37 °C with shaking at 100 rpm. At fixed time points, 1 mL of solution was taken out from each tube and 1 mL of fresh solution was added, and the concentration of RA was calculated using a UV–Vis spectrophotometer at 324 nm. Each group of samples has 3 repetitions.

2.6. Electrochemical performance of hydrogel

Three different testing methods were employed to evaluate the electrochemical performance of the hydrogels. The standard Van Der Pauw four-point probe method (ST2253, China) was performed to measure the conductivity of the different hydrogel flakes (1 cm in diameter). Cyclic voltammetry (CV) measurements and electrochemical impedance spectroscopy (EIS) measurements were performed on the hydrogels at room temperature using an electrochemical workstation (CHI660D, China). A hydrogel-coated glassy carbon electrode was used as the working electrode, Hg/Hg_2Cl_2 was used as the reference electrode, platinum was used as the counter electrode, and the electrolyte was 0.1 M PBS. The voltage range is −0.6 to 0.8 V, the sweep rate is 100 mV/s, and the sweep frequency is 1 MHz to 0.01 Hz.

2.7. Mechanical properties of hydrogels

The mechanical properties of the hydrogels were tested using a Universal Materials Tester. Compression tests were performed on cylindrical (about 10 mm in height × 12 mm in diameter) samples at room temperature at a constant speed of 5 mm/min. The elastic moduli are measured from the initial slope of the compression curves in the elastic region. Each group of samples has 3 repetitions.

2.8. Rheological properties of hydrogels

The rheological properties of different hydrogels were tested at 37 °C using a HAAKE Rehostress RS6000 rheometer. Briefly, 400 μL of OGD, OGDR, OGDP, and OGDPR hydrogels were applied to the rheometer respectively, and the upper plate was lowered to a gap size of 1 mm to test the storage modulus (G′) and loss modulus (G″) (0–15 min, 1 Hz). The shear-thinning properties of the hydrogels were determined as a function of shear rate (1 s^{-1}–100 s^{-1}). Strain sweeps (strain range:

0.1%–1000%) record the critical strain region (intersection of G′ and G″) of the hydrogel. The self-healing performance of the hydrogels were tested by three cycles of step strain from 1% to 500% (fixed frequency 1 Hz, 60 s each interval).

2.9. In vitro cytotoxicity

2.9.1. In vitro cell viability

The viability and proliferation of rat embryonic cardiomyocytes (H9C2) and rat cardiac fibroblasts (RCF) were detected by CCK-8 method. H9C2 and RCF cells were seeded into 96-well plates and incubated at 37 °C in a humidified atmosphere of 5% CO_2 for 24 h before all medium was aspirated and 100 μL of hydrogel extract was added. After continued incubation with the hydrogel extract medium for 24 h, 48 h, and 72 h, the medium was aspirated and fresh medium with 10% CCK-8 was added to each well and incubated for an additional 1.5 h. The absorbance was measured at 450 nm using a microplate reader. Media-treated cells served as a control, and relative cell viability was calculated as follows:

$$\text{Cell viability } (\%) = \frac{\text{AbS}_{\text{extract}}}{\text{AbS}_{\text{control}}} \times 100\%$$

where $\text{AbS}_{\text{control}}$ and $\text{AbS}_{\text{extract}}$ are the absorbance of cells cultured in DMEM and hydrogel extract, respectively.

The MTT assay was also used to assess cell viability in vitro according to a previous method [34].

2.9.2. Live/dead cell staining

Qualitative assessment of cell viability using live/dead cell staining. H9C2 and RCF cells were seeded into well plates and incubated at 37 °C in a humidified atmosphere of 5% CO_2 for 24 h before all medium was aspirated and 500 μL of hydrogel extract was added. After continued incubation with hydrogel extract medium for 24 h, 48 h, and 72 h, the cell plates were removed, the cells were gently washed with PBS, and then stained with PBS staining solution containing calcein and propidium iodide for 15 min at room temperature before filming under a fluorescence microscope (Olympus, Japan).

2.10. Cytoprotective effects against oxidative stress

To mimic ROS damage to cardiomyocytes in vivo, H9C2 cells were treated with a series of different concentrations of H_2O_2 (0, 50, 100, 150, 200, 300, 400, and 500 μM) for 24 h at 37 °C. Meanwhile, in order to evaluate the effect of hydrogels in protecting cardiomyocytes against oxidative stress, H9C2 cells were co-incubated with 200 μM H_2O_2 and 100 μL different hydrogel extracts for 24 h, and 200 μM vitamin C (VC) was used as a positive control, and then CCK-8 was used to measure the cell viability of each group.

2.11. Macrophage polarization assessment

RAW 264.7 cells were used as a macrophage model. The inflammatory state was induced using lipopolysaccharide (LPS) as an activator. Subsequently, cells were co-incubated with different hydrogel extracts for 24 h. Immunofluorescence staining and flow cytometry analysis were performed on RAW 264.7 cells. M1 and M2 macrophages were labeled with CD86 and CD206, respectively.

2.12. Wound scratch assay

Human umbilical vein endothelial cells (HUVECs) were inoculated in 12-well plates, and after 24 h of culture, the cells were scratched with the tip of a pipette. Then, wash twice with PBS. The hydrogel was incubated in high-glucose DMEM medium (pH 7.4) at 37 °C for 24 h to prepare the hydrogel extract. Subsequently, different hydrogel sample extracts were incubated with HUVECs. The scratch size of HUVECs was recorded at fixed time points (0, 6, 12, and 18 h). The migration rate was defined as the ratio of the healing area to the initial scratch area.

2.13. Tube formation assay

Introduce 50 μL of Matrigel into a pre-chilled 96-well plate using a chilled pipette tip and incubate for 30 min in a cell culture incubator. HUVECs were inoculated on Matrigel containing 100 μL of culture solution, and the culture medium, OGD, OGDR, OGDP, and OGDPR hydrogel extract were added respectively. After culturing for 4 h, the images were observed under a microscope. The number of nodes, number of junctions, and number of branches were calculated by ImageJ software.

2.14. Establishment of acute rat MI model and in vivo hydrogel injection

Rats were mechanically ventilated and anesthetized. A left thoracotomy was performed to expose the heart, and the left anterior descending coronary artery was ligated with suture to cause MI. On day 2 after modeling, echocardiography was performed on the surviving rats. Rats with fractional shortening (FS) $< 30\%$ were screened as follow-up experimental animals and randomly divided into saline group, OGD group, OGDR group, OGDP group, and OGDPR group. The heart was re-exposed through a second thoracotomy, and the area of MI was a gray area on the anterior wall of the LV. In order to increase the hydrogel injection volume and make the hydrogel more evenly distributed in the myocardium, 100 μL of saline, OGD, OGDR, OGDP, and OGDPR hydrogel were injected into multiple injection sites in and around the infarct area. The sham group received only a second thoracotomy, followed by suturing.

2.15. Echocardiographic evaluation of LV function

The LV function of all grouped animals was evaluated using Vevo 3100 ultrasound imaging system (Visual Sonics, Canada). Rats were anesthetized, and echocardiograms were performed 2 days after ligation (baseline, before injection), 2 and 4 weeks after treatment. Ejection fraction (EF), FS, LV internal dimensions at end-systole (LVIDs), LV internal dimensions at diastolic (LVIDd), end-systolic volume (ESV), and end-diastolic volume (EDV) were measured. All measurements are the average of three consecutive cardiac cycles.

2.16. Electrocardiogram (ECG) evaluation

Four weeks after operation, the ECGs of each group were recorded using the BL-420 N biological signal acquisition and analysis system. The QRS interval (the QRS interval refers to the distance from the Q wave to the S wave) and the QT interval (the QT interval refers to the distance from the Q wave to the T wave) among the groups were compared.

2.17. Programmed electrical stimulation (PES)

According to the previous method [34], a standard clinical PES protocol was performed 4 weeks after treatment to determine the arrhythmia inducibility. The susceptibility to arrhythmia was assessed by the induction quotient, the higher the score, the easier it is to induce arrhythmia.

2.18. Cardiac tissue resistivity measurements

At the end of 4 weeks of treatment, the animals were sacrificed to harvest the heart, and the electrical resistance of the scar tissue was measured in vitro immediately by the four-probe method.

2.19. Pathological analysis

Four weeks after injection, rats were euthanized and hearts were harvested and fixed with 4% paraformaldehyde. The hearts were subsequently embedded in paraffin, and sections (5 μm thickness) from the apex to the ligation site (1.5 mm intervals) were prepared for Masson's trichrome staining. LV wall thickness was determined as the mean minimum infarct LV wall thickness of all hearts in each group. Infarct size was defined as the ratio of the inner circumference of the infarct tissue to the entire inner circumference of the LV. The area of fibrosis was determined as the ratio of the area of collagen fibrous tissue to the area of the high-power field image. Hematoxylin-eosin (H&E) staining was used to detect the histological morphology of the infarct heart and the toxicity of other organs.

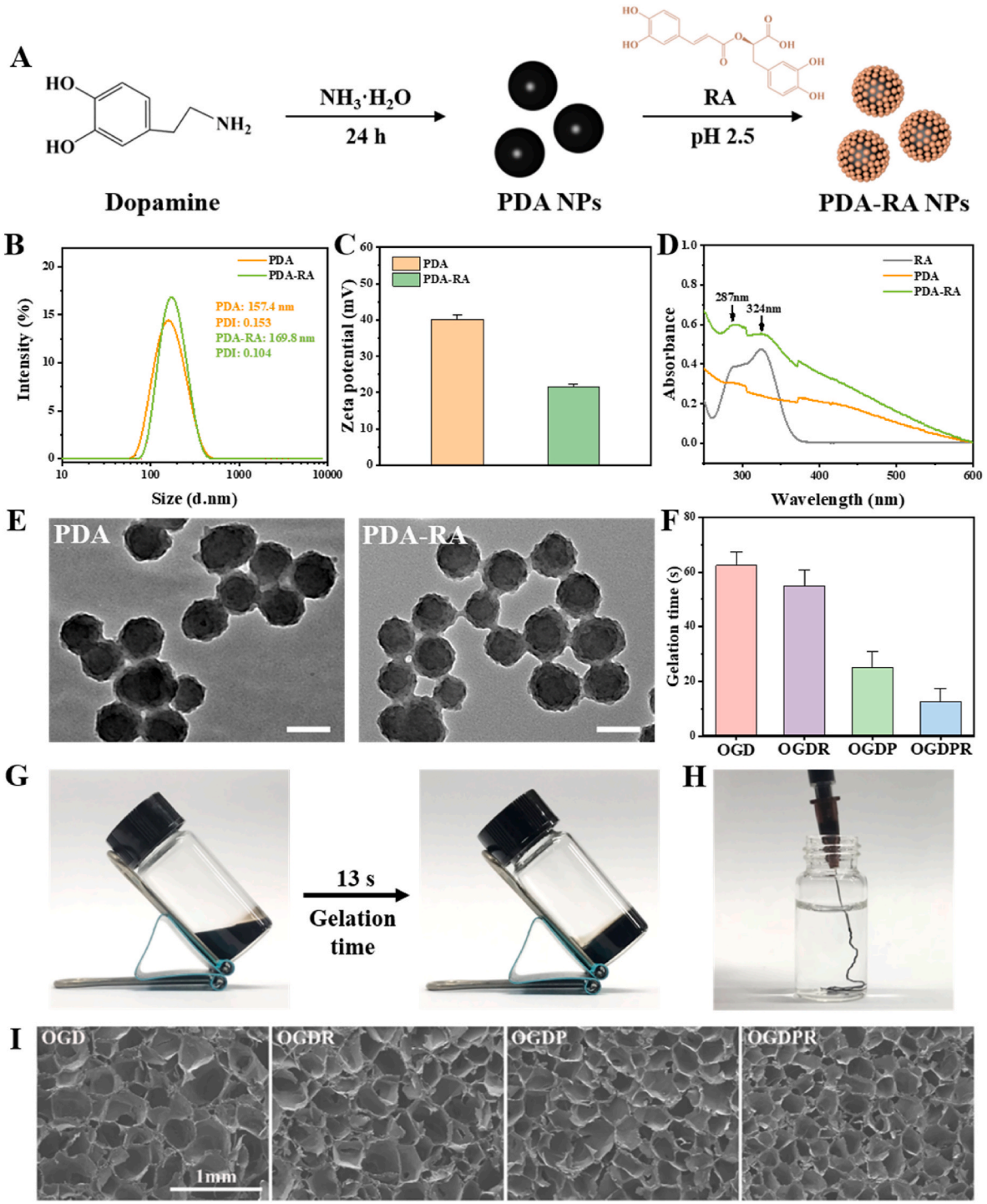

Fig. 1. Preparation and characterization of the nanoparticles and hydrogels. (A) Synthesis of PDA and PDA-RA NPs. (B, C) Particle size distribution (B) and zeta potential (C) of PDA and PDA-RA NPs. (D) UV absorption spectra of RA, PDA, and PDA-RA NPs. (E) TEM images of PDA and PDA-RA NPs. Scale bars: 100 nm. (F) Gelation time of different hydrogels. (G) Photographs of the OGDPR hydrogel before (left) and after (right) gelation. (H) Photograph of the injectability of the OGDPR hydrogel. (I) SEM images of different hydrogels. Scale bar: 1 mm.

2.20. Immunofluorescence assessment

ROS staining was used to assess ROS levels at the MI site. Terminal dexynucleotidyl transferase-mediated dUTP nick end labeling (TUNEL) staining was used to detect cell apoptosis at the MI site. CD86 and CD206 staining were used to detect the inflammatory in the infarct area. Cell proliferation at the infarct area was assessed with Ki67. Neovascularization was evaluated with α-smooth muscle actin (α-SMA) and von Willebrand factor (vWF). Connexin-43 (CX-43) and α-actinin were stained as specific markers to evaluate the recovery of cardiac function after hydrogel injection. All images were quantitatively analyzed using ImageJ software.

2.21. Statistical analysis

All data are presented as mean ± standard deviation and analyzed by one-way ANOVA and *t*-test using GraphPad Prism 8.0. $P < 0.05$ was set as the threshold for statistical significance.

Details of other experimental methods can be found in supporting information.

3. Results and discussion

3.1. Preparation and characterization of PDA-RA NPs

PDA is formed by the oxidative polymerization of dopamine. PDA contains functional groups such as catechol, amine, and imine groups. Abundant functional groups provide multiple drug loading mechanisms, such as chemical bonding (Schiff base reaction and Michael addition) and physical bonding (hydrogen bonding and π-π stacking). Under acidic conditions, PDA is positively charged, which can electrostatically adsorb negatively charged RA (Fig. 1A). We compared the drug loading and drug encapsulation efficiency under different feed ratios m(PDA/RA) under the acidic condition of pH 2.5. As shown in Table S1, as the feed ratio decreased, the drug loading of nanoparticles gradually increased, and the encapsulation first increased and then decreased. Considering the drug loading and encapsulation efficiency comprehensively, m (PDA/RA) = 2:1 was selected in this study, the drug loading was 24.06%, and the encapsulation efficiency was 63.42%.

The particle size was measured by dynamic light scattering (DLS), as shown in Fig. 1B. The sizes of PDA NPs and PDA-RA NPs are 157.4 nm and 169.8 nm, respectively. The polydispersity (PDI) is all less than 0.2, indicating that the prepared nanoparticles have good dispersion and uniformity. We also found that the two nanoparticles before and after drug loading presented different surface charges in pH 2.5 aqueous solution (Fig. 1C). The zeta potential of PDA nanoparticles was 40.2 mV, which decreased to 21.5 mV after RA loading, which indicated that positively charged PDA effectively adsorbed negatively charged RA, and PDA-RA NPs were successfully prepared. Finally, through ultraviolet detection, it was found that the PDA-RA NPs had the same ultraviolet absorption peaks as PDA and RA at 287 nm and 324 nm (Fig. 1D), indicating that the PDA-RA NPs were successfully prepared. Subsequently, transmission electron microscopy (TEM) was used to observe the morphology of nanoparticles before and after drug loading (Fig. 1E), and the results showed that both nanoparticles were spherical and uniform in size.

3.2. Preparation and characterization of the multifunctional hydrogels

The preparation and characterization of polymers are shown in Fig. S1 and Fig. S2. The aldehyde group and phenylboronic acid group on OXP can undergo Schiff base reaction and borate reaction with amino group on gelatin and amino group and catechol group on GD, respectively. OGD double network hydrogels were constructed by mixing OXP, gelatin, and GD. According to previous studies, 3 wt% of GP can endow the hydrogel with good electrochemical and mechanical properties [34]. Therefore, GP was added to the OGD gel system at a concentration of 3 wt% to form OGDP hydrogel. PDA-RA NPs was added to the OGD and OGDP gel systems at a final concentration of 0.2 wt%, forming OGDR and OGDPR hydrogels, respectively. The toxicity and antioxidant effects of OGDR and OGDPR hydrogels are shown in Fig. S3 and Fig. S4. Table S2 shows the composition of various hydrogels. The infrared spectrum of the hydrogel is shown in Fig. S5. The gelation time of the prepared hydrogel was studied by the "inverted bottle method". As shown in Fig. 1F, OGD can rapidly gelation around 60 s under the dual action of Schiff base reaction and borate reaction. With the addition of PDA-RA NPs and GP, more hydrogen bonds, boronic ester bonds and electrostatic interactions were introduced, resulting in faster gelation of OGDR, OGDP and OGDPR, up to 13 s at the fastest (Fig. 1G), while maintaining its injectability (Fig. 1H). The cross-sectional morphology of OGD, OGDR, OGDP, and OGDPR hydrogels was studied by scanning electron microscopy (SEM; JSM-7500F, JEOL, Japan) testing. As shown in Fig. 1I, the SEM images show that each group of hydrogels presents an interconnected porous structure, and the pore size is related to crosslink density. The porous structure of the hydrogel facilitates the transport of oxygen and nutrients, facilitating cell ingrowth. The pore size of OGD, OGDR, OGDP, and OGDPR hydrogels decreased sequentially, which was due to the denser polymer network due to hydrogen bonds, boronic ester bonds, and electrostatic interactions generated by the introduction of PDA-RA NPs and GP.

3.3. In vitro properties of hydrogels

Injectable hydrogels offer spatiotemporal control of therapeutic drug release through drug diffusion and material degradation. Porosity and microstructural morphology have a strong influence on drug diffusion rates through hydrogel networks or water-filled pores. As shown in Fig. 2A, all hydrogels reached swelling equilibrium within 96 h. With the increase of crosslink density, the swelling ratio of hydrogel decreases gradually. OGDPR has the smallest swelling ratio and OGD has the largest swelling ratio, and the low to moderate swelling behavior and network characteristics of the hydrogel provide potential benefits for its effective use in closed in vivo environments. Considering the existence of double cross-link network formed by double dynamic Schiff base bonds and boronic ester bonds, both imine and borate bonds can be hydrolyzed under acidic conditions, while the borate ester bond can be broken in response to ROS. The verification results of the pH and ROS dual responsiveness of the hydrogel are shown in Fig. S6. Fig. 2B and C shows the release behavior of RA in two hydrogels. Under the same time and conditions, the release rate of RA from OGDR hydrogel was significantly faster than that of OGDPR hydrogel. We speculate that this may be due to the higher crosslink density, smaller hydrogel pore size, and slower drug diffusion in the gel network of OGDPR compared with OGDR. Interestingly, OGDR and OGDPR hydrogels released the fastest in pH 5.0 and 200 μM H_2O_2 compared to pH 7.4 or single environment (pH 5.0 or 200 μM H_2O_2). This is mainly due to the dual responsive behavior of the hydrogel to pH and ROS. Rapid breakdown of chemical bonds within the hydrogel under acidic and oxidative conditions resulted in accelerated release of RA.

The rheological properties of the hydrogels were tested using a rotational rheometer. The gelation kinetics evaluated in the dynamic time-scanning mode are shown in Fig. 2D, and the storage modulus (G′) values of all the hydrogels are greater than the loss modulus (G″) value, indicating that all hydrogels can rapidly form stable cross-linked structure. In addition, as the cross-link density increases, the G′ and G″ values of the hydrogel also gradually increase. As the shear rate increases, the hydrogel exhibits shear-thinning properties (Fig. 2E). Strain scans (Fig. 2F) showed that all hydrogels remained stable under low strain. As the strain increases above the critical value (G′ is lower than G″), the hydrogel network collapses and the solid hydrogel transforms into a fluid state. This change is attributed to the cleavage of Schiff base bonds and separation of boronic ester bonds under high shear strain. In

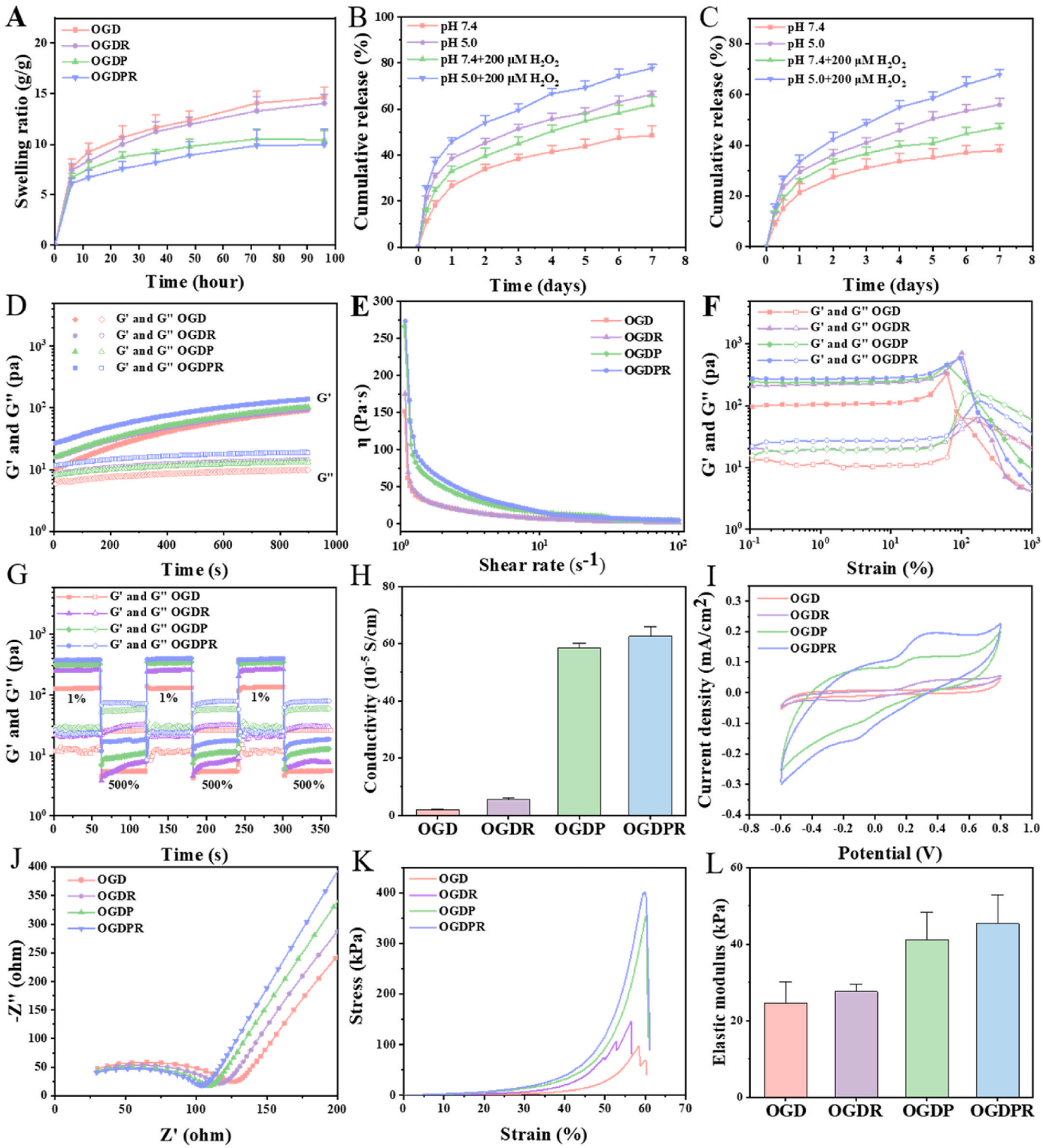

Fig. 2. Properties of multifunctional hydrogels. (A) Swelling ratio of hydrogels in PBS (n = 5). (B, C) Release profiles of RA from OGDR (B) and OGDPR (C) hydrogels under different conditions (n = 3). (D) Rheological measurements of hydrogels in time-sweep mode. (E) Viscosity of hydrogels as a function of shear rate. (F) G′ and G″ of the hydrogels under different oscillatory strains. (G) Self-healing properties of hydrogels under alternating strain. (H) Conductivity of different hydrogels (n = 3). (I, J) CV curves (I) and EIS (J) curves of different hydrogels. (K, L) Stress-strain curves (K) and elastic moduli (L) of the hydrogels (n = 3).

alternating strain scans (Fig. 2G), all hydrogels maintained a stable network structure at low strain (1%). At high strain (500%), G' < G″ indicates that the hydrogel crosslinking network collapses. After stepping from high strain to low strain, both G′ and G″ quickly returned to their initial values, suggesting the recovery of the crosslinked network of the hydrogel, indicating that the hydrogel has good self-healing properties. The shear-thinning properties and rapid network healing ability of hydrogels allow for their injection and rapid recovery.

PPy has excellent conductivity, and the conductivity of hydrogel is crucial for the transmission of electrical signals in infarcted

myocardium. Firstly, we measured the conductivity of the hydrogel using a four-point probe (Fig. 2H). The conductivities of OGD and OGDR hydrogels without conductive component GP were 2.02×10^{-5} S/cm and 5.71×10^{-5} S/cm, respectively. After adding GP, the conductivities of OGDP and OGDPR hydrogels were respectively increased to 5.86×10^{-4} S/cm and 6.27×10^{-4} S/cm, which is consistent with the conductivity range of native cardiac tissue (approximately 10^{-4} S/cm) [35]. Subsequently, electrochemical studies were performed using an electrochemical workstation with a three-electrode system. The CV curve (Fig. 2I) of the hydrogel presents a symmetrical hysteresis loop and a pair of redox peaks. With the addition of GP, the area of the hysteresis loop increases and the redox peak becomes more obvious. The EIS curves (Fig. 2J) show that OGDP hydrogels and OGDPR hydrogels containing GP have smaller semicircle diameters at high frequencies, which proves that the addition of GP improves the conductivity of hydrogels, consistent with the results of conductivity measurement and CV curve analysis. Excellent electrical conductivity makes it more suitable for the repair of heart tissue.

The mechanical stiffness and elasticity of the hydrogels were tested by stress-strain curves, and it was found that all hydrogels were relatively rigid, flexible, and mechanically elastic at the same time (Fig. 2K). The elastic modulus of hydrogel increases with the increase of cross-linking density. OGDPR hydrogel shows the highest elastic modulus (45.35 kPa) (Fig. 2L), which matches the elastic modulus of native myocardium (11.9–46.2 kPa [36]), and is suitable for use as a biological material to support cardiac contraction.

3.4. In vitro and in vivo biocompatibility evaluation of hydrogels

The cytocompatibility and cytotoxicity of the hydrogels were evaluated using H9C2 and RCF cells. The results of the live/dead cell staining qualitative test in Fig. 3A show that the cells in each hydrogel treatment group are basically in a viable state (green dots), and only a small number of negligible dead cells (red dots) appear, indicating that they are growing well. And with the prolongation of time, the number of viable cells in the field of view gradually increased, indicating that the hydrogel has good cytocompatibility and promotes cell proliferation. Quantitative analysis of CCK-8 cell viability at 24, 48, and 72 h compared to the control group showed that all hydrogels did not affect the viability of H9C2 and RCF cells (Fig. 3B and C). With the prolongation of the culture time, the cell viability decreased slightly, but the cell viability of all groups was greater than 80% after 72 h of culture. MTT also showed similar results (Fig. S7), indicating that all hydrogels had good biological safety and were suitable for in vivo application. In addition, the hydrogel has good blood compatibility (Fig. S8) and degradability (Fig. S9 and Fig. S10) and injection into the body will not cause damage to liver and kidney functions (Fig. S11).

3.5. Antioxidant and macrophage phenotype regulation effect of hydrogel

The hydrogel has a good ability to scavenge DPPH, ·OH, and $O_2^{\bullet-}$ free radicals (Fig. S12), and exhibits good antioxidant effect. In addition, H_2O_2 is a common ROS. Therefore, H_2O_2-induced cellular oxidative stress has been extensively studied. H_2O_2 was used to induce oxidative stress in H9C2 cells, and the ability of hydrogels to protect cardiomyocytes against oxidative stress was evaluated. The results in Fig. 3D show that all hydrogel-treated groups had increased cell viability compared to the H_2O_2 control group. In particular, the OGDPR hydrogel group showed significantly higher cell viability than the other groups, which is consistent with its highest DPPH clearance efficiency in vitro. These results indicated that the boronic ester bond-based hydrogels had certain antioxidant capacity, while the antioxidant capacity of OGDR and OGDPR hydrogels was further enhanced, which may be related to the excellent antioxidant activity of RA.

Phenotypic changes in macrophages play a key role in tissue repair. Polarization of macrophages from a pro-inflammatory M1 phenotype to an anti-inflammatory or pro-healing M2 phenotype is beneficial in attenuating chronic inflammation and fibrosis. To investigate the effect of hydrogel on macrophage polarization, we first performed in vitro macrophage immunofluorescence staining assay. As shown in Fig. 3E, the expression of CD86 in RAW264.7 cells treated with LPS was significantly increased, while the expression of CD86 showed varying degrees of decrease after treatment with hydrogel extract, while the expression of CD206 was upregulated. Especially RA-containing OGDR and OGDPR hydrogels exhibited significant downregulation of CD86 expression and upregulation of CD206 expression, which was attributed to the powerful anti-inflammatory effect of RA. Further evaluation by flow cytometry yielded similar results (Fig. 3F–H). The above results prove that the prepared hydrogel can effectively promote the conversion of macrophages from the M1 phenotype to the M2 phenotype, and promote the resolution of inflammation and tissue repair after MI.

3.6. Multifunctional hydrogel promotes endothelial cell proliferation, migration, and tube formation

Effective myocardial repair after MI usually requires a strong angiogenic reaction, which starts from the marginal zone and extends to the center of the infarcted area, and then quickly forms a dense capillary network to promote gas exchange, nutrient diffusion, and waste transport to meet the infarct sites of high metabolic needs and prevent the continued death of cardiomyocytes at the infarct margin [37]. Vascularization of endothelial cells is a very important process in angiogenesis [38]. To test whether the hydrogel has any functional role in angiogenesis, we examined the effect of the hydrogel on endothelial cells. Its biological activity on HUVECs was investigated by several different but complementary methods including proliferation assay, scratch assay and tube formation assay. First, the effect of the hydrogel on endothelial cell proliferation was evaluated by a CCK-8 cell proliferation assay. The results showed that all hydrogel groups had varying degrees of endothelial cell proliferation-promoting effects over time, among which OGDP and OGDPR hydrogels had more significant endothelial cell proliferation-promoting effects (Fig. S13). Then, the effect of the hydrogel on endothelial cell migration was assessed. The scratch test is a simple, low-cost in vitro assay of cell migration. At 6 h, cell migration could be clearly observed in all hydrogel groups, which was significantly different from the control group (Fig. 4A). In addition, complete cell migration was observed at 18 h for all scratches in the OGDPR group, while large non-migrated areas remained in the control group. The quantitative results (Fig. 4B) were consistent with the observations, and there was a significant difference in cell migration between the OGD group and the OGDPR group, which may be attributed to the role of PPy in promoting endothelial cell proliferation and migration [39]. Therefore, the angiogenic ability of the hydrogel was tested by HUVECs tube formation assay. After 4 h of culture, various degrees of angiogenesis were observed in all groups (Fig. 4C). The number of nodes, junctions, and branches were obtained by quantifying tube formation images (Fig. 4D–F). The results showed that OGDPR hydrogels greatly promoted tube formation of endothelial cells compared with control and GP-free hydrogels, which is consistent with reports that PPy promotes angiogenesis in vitro [39].

3.7. Multifunctional hydrogel improves cardiac function

Given the good performance and biocompatibility of hydrogels in vitro, we set out to examine the therapeutic effect of a drug-loaded injectable conductive hydrogel system in alleviating pathological LV remodeling in a rat model of MI. Fig. 5A shows important time points of animal experiments. Ligate the anterior descending branch of the left coronary artery to establish a rat MI model, and the obvious ST-segment elevation in the ECG confirmed the success of the model (Fig. 5B). In addition, echocardiography was used to screen MI rats with FS $< 30\%$ two days after modeling to ensure the consistency of initial injury in

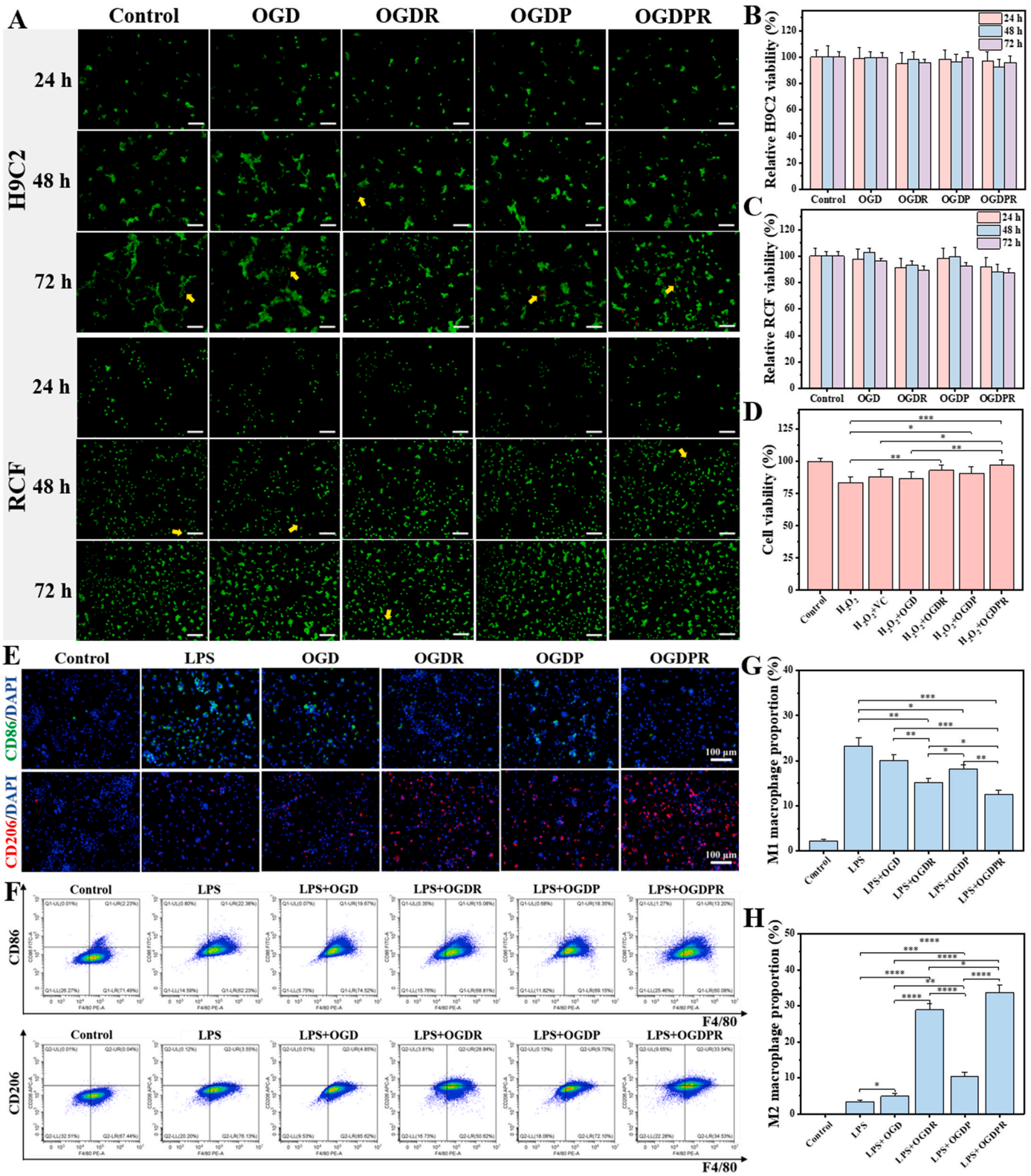

Fig. 3. In vitro cytocompatibility and antioxidant activity of hydrogels. (A) Live/dead staining of H9C2 and RCF incubated with different hydrogel extracts. Green dots: living cells; red dots: dead cells. Yellow arrows indicate dead cells. Scale bars: 100 μm. (B, C) CCK-8 assay for cell viability of H9C2 (B) and RCF (C) co-incubated with hydrogel extracts, untreated cells were used as control (n = 6). (D) Cell viability of H9C2 cells treated with H_2O_2 (200 μM) and different hydrogel extracts for 24 h (n = 5). (E) Images of CD86 and CD206 immunofluorescent staining in macrophages stimulated with LPS and treated with different hydrogel extracts. (F–H) Representative flow cytometry analysis images (F) of different groups and the proportion of M1 (G) and M2 (H) macrophages (n = 3). *P < 0.05, **P < 0.01, ***P < 0.001, ****P < 0.0001.

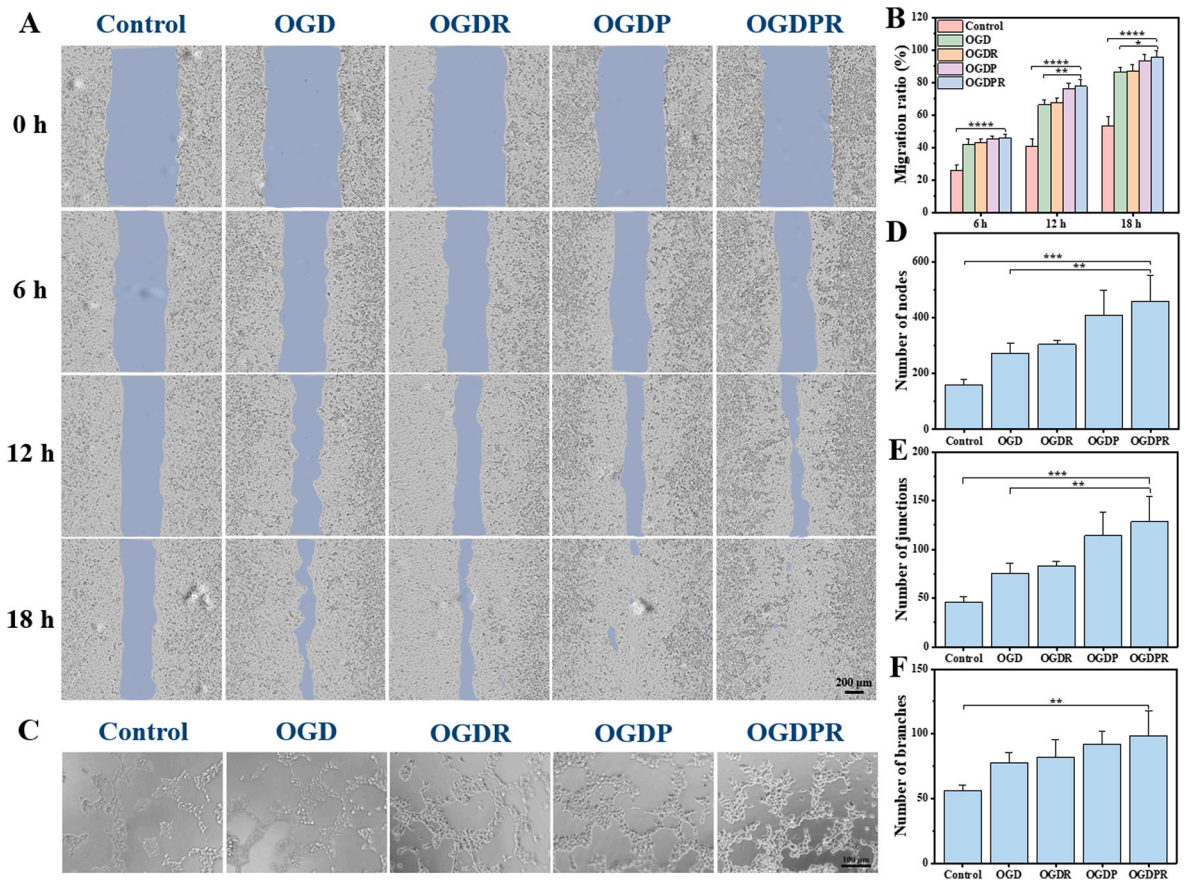

Fig. 4. Hydrogels promote HUVECs migration and tube formation. (A) Representative images of HUVECs cultured with different hydrogel extracts for 0, 6, 12, and 18 h. Scale bar: 200 μm. (B) Quantitative results of wound cell migration at different time points (n = 3). (C) Images of HUVECs forming tubes in vitro. (D–F) Quantitative results of the number of nodes (D), the number of junctions (E), and the number of branches (F) of different hydrogel groups (n = 4). Scale bar: 100 μm *P < 0.05, **P < 0.01, ***P < 0.001, ****P < 0.0001.

each group (Fig. 5C). In this experiment, MI model rats were treated with saline, OGD hydrogel, OGDR hydrogel, OGDP hydrogel, and OGDPR hydrogel, respectively (Fig. 5D).

Echocardiography was performed to record the cardiac function of the rats in each group 2 days after modeling, 2 and 4 weeks after treatment. The results are shown in Fig. 5E and F, where the initial cardiac function was significantly reduced and at the same level in the saline and hydrogel groups compared with the sham group. These results indicated that all groups of rats had the same degree of initial MI injury, resulting in reduced contractility of the LV myocardium. After 2 weeks of treatment, echocardiography showed a significant decrease in EF and FS, as well as a significant increase in LVIDs, LVIDd, ESV, and EDV in the saline group compared to the sham group, indicating that severe infarct expansion and LV remodeling occurred in the saline group. The EF and FS of all hydrogel-treated rats were higher than those of saline group. The cardiac function of rats in the non-conductive and non-drug-loaded OGD hydrogel group also improved, which may be related to the physical support of the hydrogel itself and its weak ROS scavenging ability. Meanwhile, the EF and FS of OGDR and OGDP hydrogels were improved compared with those of OGD hydrogel group, proving that PDA-RA NPs and conductive material GP have a certain therapeutic effect on MI tissue repair. Most importantly, the treatment effect of OGDPR hydrogel group was the best, indicating that the synergistic effect of PDA-RA NPs with conductive material GP could better protect cardiac function. Echocardiography at 4 weeks showed that the cardiac function of the saline group was further reduced, and the cardiac function of all hydrogel treatment groups was further improved, indicating that the treatment effect of the hydrogel group was getting better. The video of echocardiogram clearly presented that the OGD, OGDR, OGDP, and OGDPR groups had successively thickened infarct walls and successively improved ventricular wall movement compared to the saline group, with the OGDPR group showing the best cardiac function (Video S1).

Supplementary video related to this article can be found at https://doi.org/10.1016/j.bioactmat.2023.07.007

3.8. Protection of cardiac electrophysiology by multifunctional hydrogels

Researches have shown that restoration of conductivity in the area of MI is crucial for the recovery of cardiac function [40]. Conductive biomaterials have been reported to connect normal and infarcted areas, respond to electrical signals in a timely manner, and improve the conductivity of scar tissue. They prevent arrhythmias, promote synchronized contraction, and improve cardiac function [41]. In vitro experiments have demonstrated that the hydrogel has good electrical conductivity. Therefore, we further verified the effect of the hydrogel on the electrophysiological properties of the MI region. ECG analysis showed that due to severe myocardial tissue necrosis and fibrosis after MI, significant ST segment elevation and pathological Q wave appeared in the saline group (Fig. 6A), and the QRS and QT interval were significantly prolonged (Fig. 6C and D). OGDR and OGDP groups had no pathological Q waves, and the ST segment decreased, indicating that the effective inhibition of pathological ROS generation, reduction of cell apoptosis, and restoration of electrical conduction in the infarct area can increase the transmission efficiency of electrical pulse signals after MI. Likewise, the OGDPR hydrogel-treated group had normalized ECG

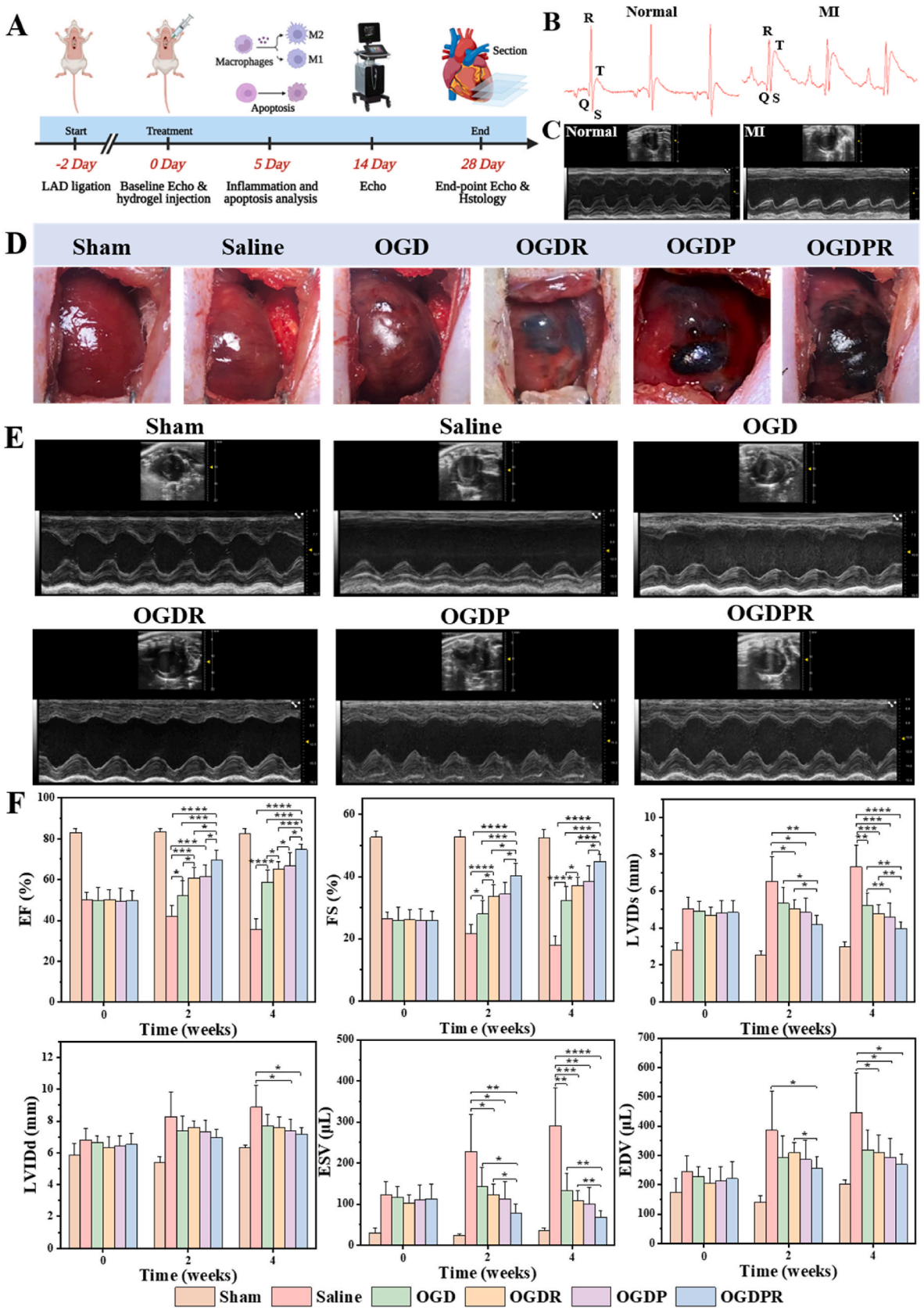

Fig. 5. Injection of hydrogel after MI improves cardiac function. (A) Critical time points of animal experiments. (B) ECG before (left) and after (right) modeling. (C) Echocardiograms before (left) and after (right) modeling. (D) Gross pictures of rat hearts injected with different biomaterials. (E) Representative echocardiographic images of each group at 4 weeks after injection. (F) Cardiac function indicators were determined by echocardiography after 0 (before injection), 2, and 4 weeks of treatment (n = 6). *P < 0.05, **P < 0.01, ***P < 0.001, ****P < 0.0001.

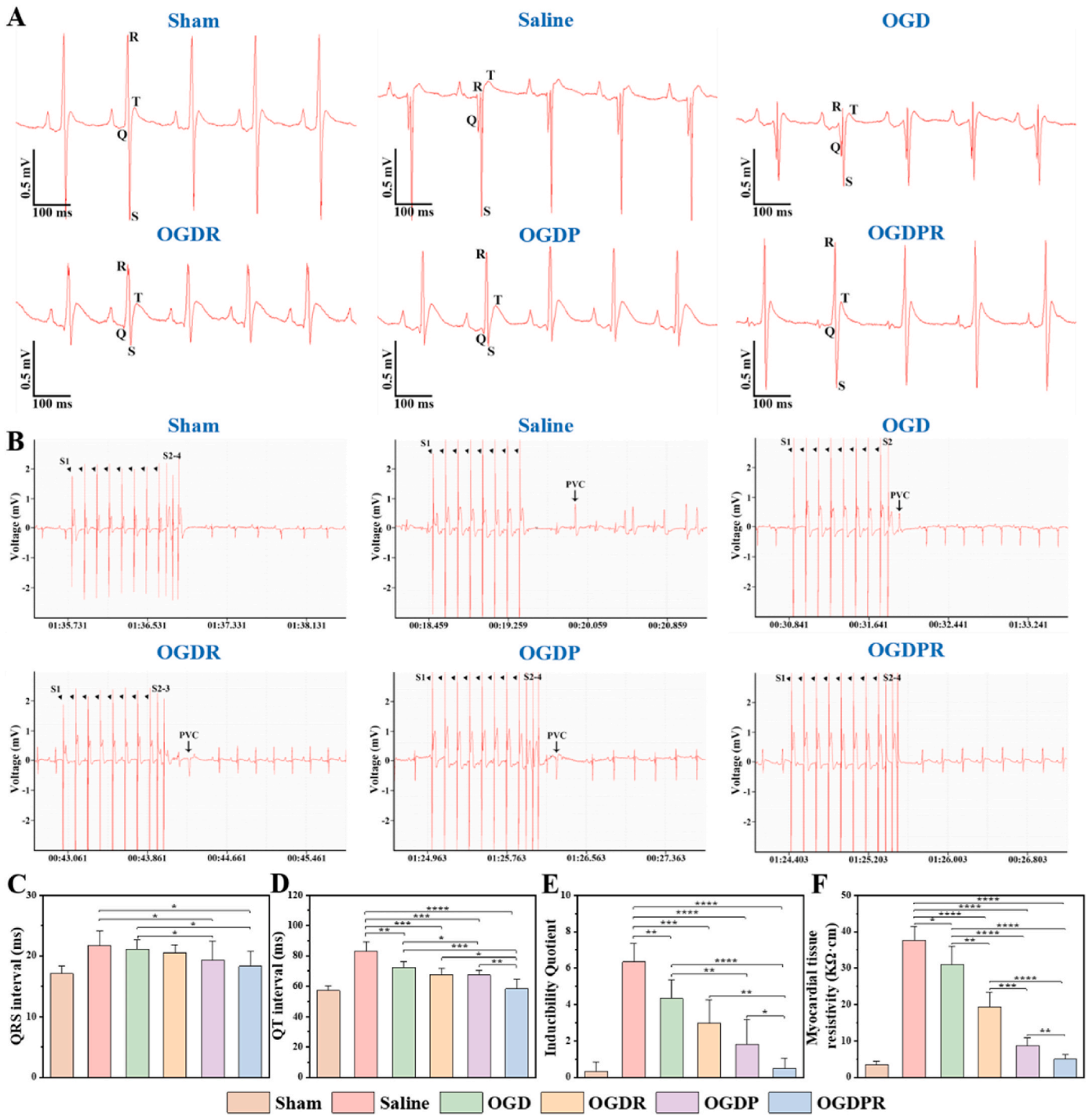

Fig. 6. Protective effects of hydrogels on the electrophysiology of infarcted hearts. (A) ECG of each group 4 weeks after treatment. (B) ECG of arrhythmias induced by PES 4 weeks after injection. (C, D) Effects on QRS (C) and QT (D) intervals after injection of different biomaterials (n = 6). (E) Arrhythmia susceptibility characterized by inducibility quotient (n = 6). (F) Tissue resistivity of the infarct scar areas (n = 6). *P < 0.05, **P < 0.01, ***P < 0.001, ****P < 0.0001.

waveforms and exhibited the most significantly improvement in QRS and QT interval, which was almost identical to the sham group. The research results confirmed that the RA-loaded conductive hydrogel OGDPR restored the electrical conduction from the scar area to the healthy area while scavenging ROS and inhibiting cell apoptosis, activated the surviving cardiomyocytes to generate normal action potentials, and significantly improved the transmission of electrical impulse signals in the infarcted myocardium, thereby better repairing cardiac function.

Researches have shown that weakly excitable scar tissue in the infarcted area can block the conduction of electrical signals in non-infarcted myocardium, which may lead to ventricular arrhythmias. In order to determine whether injection of OGDPR hydrogel could effectively reduce cardiac arrhythmias, a standard clinical PES protocol was administered [34]. As shown in Fig. 6B, arrhythmias were less likely to occur in the sham group under PES stimulation. However, arrhythmia was easily induced in the saline group. Inducing arrhythmias became more difficult in the RA-loaded hydrogel OGDR and conductive hydrogel OGDP groups, indicating that they play a beneficial protective role in avoiding induced arrhythmias. OGDPR hydrogels showed the lowest

susceptibility to arrhythmias (Fig. 6E), which may be related by multiple mechanisms. OGDPR hydrogel can scavenge ROS in the infarct area and reduce cardiomyocyte apoptosis. At the same time, it improves the transmission of electrical pulses in the scar tissue, makes the surviving myocardium isolated by the scar contract simultaneously, and promotes the synchronous contraction with the normal myocardium, thereby improving heart function. Moreover, increased electrical transmission in the scar may reduce the number of unidirectional outlet blockages for electrical signals, thus reducing the likelihood of circuit formation in ventricular arrhythmias [42].

The electrical resistivity of the scar tissue in each group was measured, and it was found that these hydrogels successively reduced the electrical resistivity of the myocardial scar tissue (Fig. 6F), with the lowest resistivity in the OGDPR group, which was consistent with the highest electrical conductivity measurement of the hydrogel in vitro. The low electrical resistivity was beneficial to the conduction of cardiac electrical signals, which further confirmed the results of ECG and PES.

3.9. Effects of multifunctional hydrogels on LV remodeling after MI

Four weeks after in vivo hydrogel injection in rats, Masson's trichrome staining was used to evaluate the in vivo treatment efficiency. The saline group experienced severe MI, manifested by myocardial collapse, wall thinning, infarct fibrosis, and large areas of blue collagen deposition (Fig. 7A). Quantitative analysis (Fig. 7B–D) showed that the OGD hydrogel treatment group presented a thicker ventricular wall thickness than the saline group, and this improvement was most likely attributable to the mechanical support effect of the hydrogel, enabling it to withstand certain myocardial load. In addition, the presence of boronic ester bonds in the hydrogel helps to scavenge a part of ROS in the infarcted region, improving the microenvironment of the infarct and preventing further expansion of the infarcted area. In the OGDR hydrogel-treated group loaded with PDA-RA NPs, the area of myocardial fibrosis was significantly reduced, which was attributed to the anti-fibrotic effect of RA. The OGDP and OGDPR hydrogel treatment groups showed thicker wall thickness, which may be due to the significantly improved mechanical strength of the cross-linked network by the conductive material GP, which is consistent with its higher compressive elastic modulus in vitro and slower degradation rate in vivo. The OGDPR hydrogel treatment group showed the thickest wall thickness, the smallest infarct size and fibrosis area, significantly inhibited ventricular remodeling, and better preserving LV geometry. These findings strongly support the optimal therapeutic effect of OGDPR hydrogels on cardiac structures after MI. In addition, H&E staining showed that all hydrogel-treated rat hearts were morphologically similar to the sham-operated group after 4 weeks of treatment. No in situ inflammation or

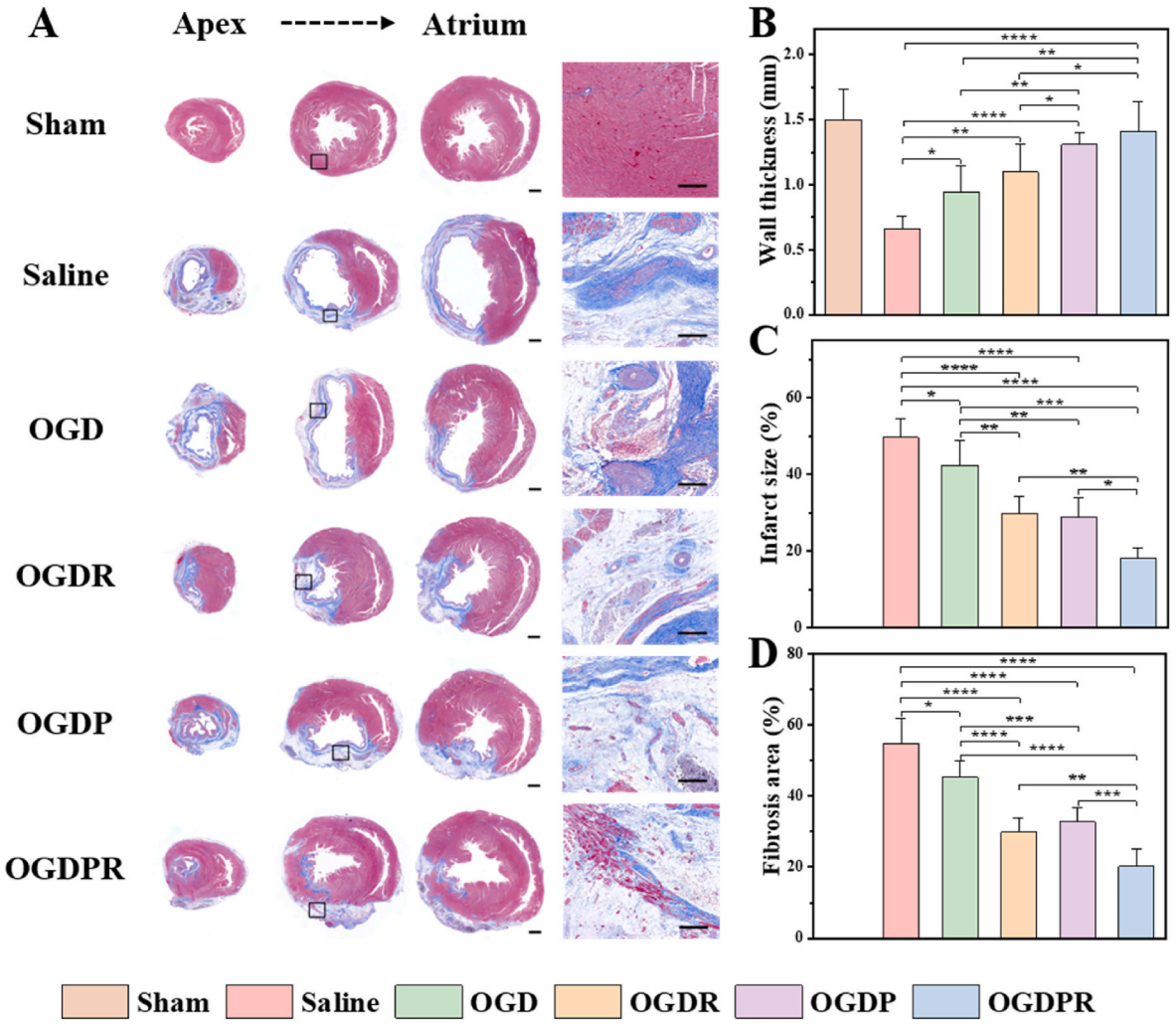

Fig. 7. Hydrogels attenuate pathological remodeling of the LV. (A) Masson's trichrome staining was performed on multiple cardiac slices from the apex to the atrium 4 weeks after treatments. The image at high magnification comes from the black box of the low magnification image. Scale bars: low magnification = 1 mm, high magnification = 200 μm. (B–D) Quantitative analysis of the wall thickness (B), infarct size (C), and fibrosis area (D) in each group after 4 weeks of treatment according to Masson's trichrome staining (n = 6). *P < 0.05, **P < 0.01, ***P < 0.001, ****P < 0.0001.

pathological changes were observed on H&E staining of other major organs (liver, spleen, lung, and kidney) (Fig. S14). All hydrogels are considered to have a good safety profile.

3.10. Effects of multifunctional hydrogel on antioxidative, anti-inflammatory, and anti-apoptosis

A good cardiac microenvironment is critical for the survival and regeneration of cardiomyocytes. The death of cardiomyocytes in the infarct area activates the inflammatory response, stimulating the recruitment and proliferation of macrophages [43]. At the same time, a large amount of ROS generated in the myocardium after MI can activate multiple pathways to produce pro-inflammatory cytokines [44]. Excessive dysregulation and prolonged inflammation disrupt cellular homeostasis and further accelerate cardiomyocyte death [45], leading to LV dilatation and systolic dysfunction [15,46]. Therefore, timely removal of ROS in the infarct area and inhibition of inflammatory responses are crucial for effective repair of damaged tissues [47,48]. With the progress of tissue repair, phenotypic changes of macrophages play a key role [49]. We first assessed whether the hydrogel could effectively reduce high ROS levels after infarction. As shown in Fig. 8A and D, compared with the sham operation group, the relative fluorescence intensity of ROS in the saline group was higher, indicating that the level of ROS increased after MI. All hydrogel-treated groups showed varying degrees of reduction in ROS levels, which was due to the ability of phenylboronic acid-based hydrogels to scavenge ROS. Due to the certain antioxidant activity of PPy, the OGDP hydrogel group showed lower ROS levels than the OGD hydrogel treatment group. At the same time, the fluorescence signal and relative fluorescence intensity of OGDR and OGDPR hydrogels were significantly reduced, indicating that RA can effectively reduce the ROS level at the MI site, which is mainly due to the antioxidant effect of RA. The ideal process for tissue repair is that macrophages can be polarized from a proinflammatory M1 phenotype to an anti-inflammatory or pro-healing M2 phenotype [17], which is beneficial for reducing chronic inflammation and fibrosis. Inflammatory M1 macrophages dominate the first three days after MI and differentiate into a reparative M2 phenotype 3–5 days after MI to prepare for tissue repair [17,46,50]. Infarcted cardiac tissue was collected 5 days after injection, and the effect of the hydrogel on the inflammatory and repair phases was assessed. We stained M2 macrophages and M1 macrophages using antibodies against CD206 (green) and CD86 (red), respectively. As shown by immunofluorescence (Fig. 8B), extensive infiltration of pro-inflammatory M1 macrophages was observed in the saline group, which had the lowest M2/M1 ratio compared with all other groups (Fig. 8E). The expression of CD206 was significantly up-regulated and the expression of CD86 was significantly down-regulated in all hydrogel treatment groups, that is, the M2/M1 ratio was increased, which was due to the fact that the phenylboronic acid-based hydrogel can scavenge ROS, thereby reducing the inflammatory response. This effect was further enhanced in the RA-added hydrogel groups (OGDR group and OGDPR group). It was shown that RA-loaded hydrogel significantly inhibited M1 polarization and promoted M2 polarization of macrophages in vivo. Inhibition of the inflammatory response can reduce cardiomyocyte apoptosis, thereby reversing the pathological remodeling of the LV. Therefore, cardiomyocyte apoptosis was assessed by TUNEL staining. As expected, the sham and saline groups had very low (0.18%) and high percentages (25.5%) of apoptotic cells, respectively (Fig. 8C and F), demonstrating the success of the MI model. All hydrogel treatment groups inhibited cardiomyocyte apoptosis, and the OGDR and OGDPR hydrogel treatment groups showed more significant effect in reducing apoptosis compared to the saline group and other hydrogel groups. This is mainly attributed to the anti-apoptotic effect of RA, which makes the hydrogel more capable of maintaining cell viability in an oxidative microenvironment. These results confirmed that OGDPR hydrogel had anti-inflammatory effects and promoted macrophage polarization to M2 phenotype in vivo, which provided a more favorable microenvironment for myocardial cells in the infarction area, reduced cell apoptosis, delayed the loss of functional cardiomyocytes in the infarct area, and was beneficial to maintaining the cardiac structure and protecting cardiac function, and promoted the treatment of MI.

3.11. Effects of hydrogels on promoting cell proliferation and angiogenesis

Next, we analyzed the effect of the hydrogel on cell proliferation in the infarct area using Ki67 immunofluorescence staining. The results (Fig. 9A and C) showed that only very few Ki67-positive cells were detected in the saline group, indicating little cell proliferation after MI. There were significantly more Ki67-positive cells in the conductive hydrogel groups (OGDP and OGDPR groups) compared to the saline and other hydrogel groups, which may be attributed to the pro-proliferative effect of the conductive polymer [51–53]. OGDPR hydrogel has a stronger effect on promoting cell proliferation and can provide functional reconstruction for damaged myocardial tissue. After MI, revascularization of the infarcted myocardium is of great significance for the recovery of cardiac function [54]. Increasing angiogenesis is an effective way to restore oxygen and nutrient supply to the infarcted area. Cardiac tissue sections were double-stained for α-SMA (marking mature arterioles) and vWF (marking microvessels) to analyze angiogenesis. As shown in Fig. 9B, at 4 weeks after treatment, there was a small amount of angiogenesis in the saline group, which may be related to active cardiac compensation. The hydrogel treatment group resulted in significantly more mature new blood vessel formation than the saline group, especially the OGDPR hydrogel group showed the most angiogenesis, due to the pro-angiogenic effect of PPy, which was consistent with the results of in vitro experiments. The quantitative analysis data of α-SMA and vWF-labeled blood vessel density in Fig. 9D and E are consistent with the results of fluorescent staining pictures. This indicates that the designed OGDPR hydrogel is very effective in promoting cardiac angiogenesis. The above results suggest that OGDPR hydrogel may be beneficial to cell proliferation, as well as recruit endothelial cells to the infarct area [40,55,56], which is beneficial to myocardial repair after MI, consistent with previous reports.

3.12. Effects of multifunctional hydrogels on the expression of cardiac-specific markers

The synchronous contraction of cardiomyocytes is mainly based on the expression of α-actinin (a cardioskeletal protein) closely related to myocardial maturation and regulation of muscle contraction. CX-43, a gap junction protein, is primarily responsible for the electrical contraction coupling of the myocardium, which is critical for coordinated myocardial function [57,58]. Here, α-actinin and CX-43 were used as cardiac-specific markers to examine cardiac function 4 weeks after hydrogel injection. As shown in Fig. 10A and C, compared with the sham group, the area coverage of α-actinin was significantly reduced in the saline group. The OGDPR hydrogel-treated group had the highest α-actinin area coverage, indicating the greatest improvement in cardiac function. CX-43 was barely expressed in the saline group, but the area coverage of CX-43 was higher in the hydrogel treatment group, especially the OGDPR hydrogel (Fig. 10B and D), indicating better electrical contraction at 4 weeks after surgery. Most importantly, the expressions of α-actinin and CX-43 in the OGDPR hydrogel group were higher than those in the OGDR hydrogel group and the OGDP hydrogel group, indicating an enhanced therapeutic effect of the synergistic therapy. These results suggest that promoting mechanical coupling or electrical signal coupling between cardiomyocytes may lead to synchronous cell contraction and promote myocardial functional recovery, which is consistent with the above functional results.

4. Conclusions

This study successfully constructed a multifunctional drug-loaded

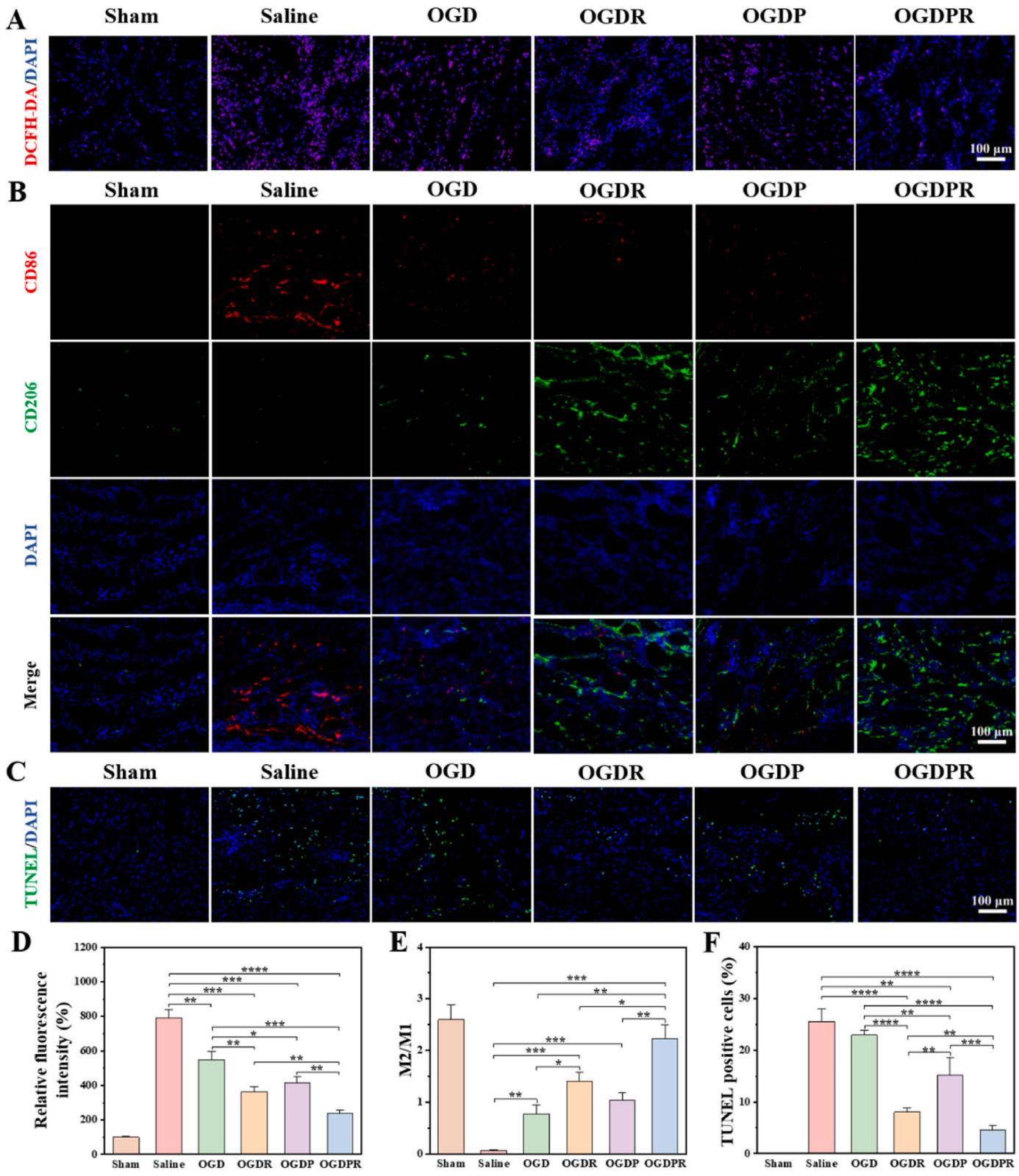

Fig. 8. Hydrogels resist oxidation, inhibit inflammation, and reduce apoptosis. (A) ROS expression in infarcted hearts after different treatments. (B) Immunofluorescence images of $CD86^{+}$ and $CD206^{+}$ macrophages in the area of MI. Scale bar: 100 μm. (C) Representative TUNEL staining images of the infarct area. Scale bar: 100 μm. (D–F) Quantitative analysis of relative ROS fluorescence intensity (D), M2/M1 ($CD206^{+}/CD86^{+}$) ratio (E), and TUNEL positive cells (F) in the infarct area of the heart (n = 4). *P < 0.05, **P < 0.01, ***P < 0.001, ****P < 0.0001.

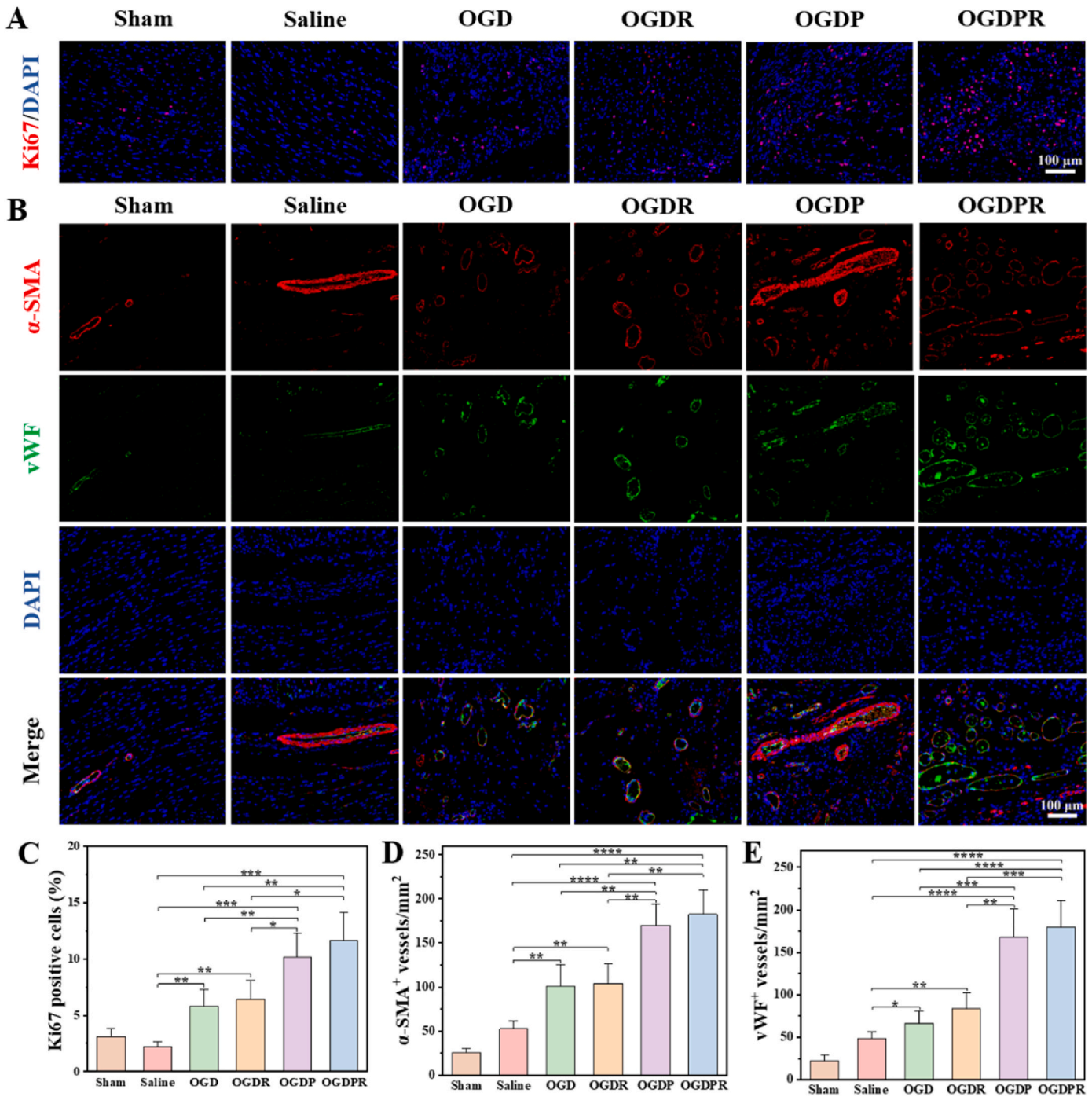

Fig. 9. Hydrogels promote cell proliferation and angiogenesis. (A) The expression of Ki67 in the MI area after 4 weeks of different treatments. Scale bar: 100 μm. (B) Representative images of α-SMA/vWF double staining in different treatment groups at 4 weeks. Scale bar: 100 μm. (C–E) Quantitative analysis of Ki67 positive cells (C), α-SMA positive vessels (D), and vWF positive vessels (E) in the infarct regions (n = 4). *P < 0.05, **P < 0.01, ***P < 0.001, ****P < 0.0001.

conductive hydrogel OGDPR that responds to the microenvironment of MI and meets the biological activity requirements of multiple stages of MI. This hydrogel combines the electrical conductivity with the anti-apoptotic, anti-inflammatory and anti-fibrotic properties of RA for the treatment of MI in rats. Boronic ester bonds enable on-demand release of RA in response to the high ROS and low pH microenvironment of MI. OGDPR hydrogels have electrical conductivity, mechanical elasticity, and biocompatibility that match those of native myocardium. The hydrogel exhibited protection against H_2O_2-induced cellular oxidative stress and promoted endothelial cell migration and tube formation. Injection of OGDPR hydrogel into the infarcted myocardium significantly restored cardiac function, increased ventricular wall thickness, and inhibited infarct expansion. On the one hand, RA released from hydrogel can remove ROS, regulate inflammatory microenvironment, inhibit cell apoptosis, and continuously inhibit myocardial fibrosis; on the other hand, PPy endows hydrogels with good electrical conductivity and recruits endothelial cells to promote new blood vessel formation. This study verified the effectiveness of a comprehensive therapeutic strategy combining mechanical support, anti-inflammation, anti-apoptosis, anti-fibrosis, and restoration of electrical signal transmission in the infarct area in one hydrogel scaffold, which has potential clinical application prospects.

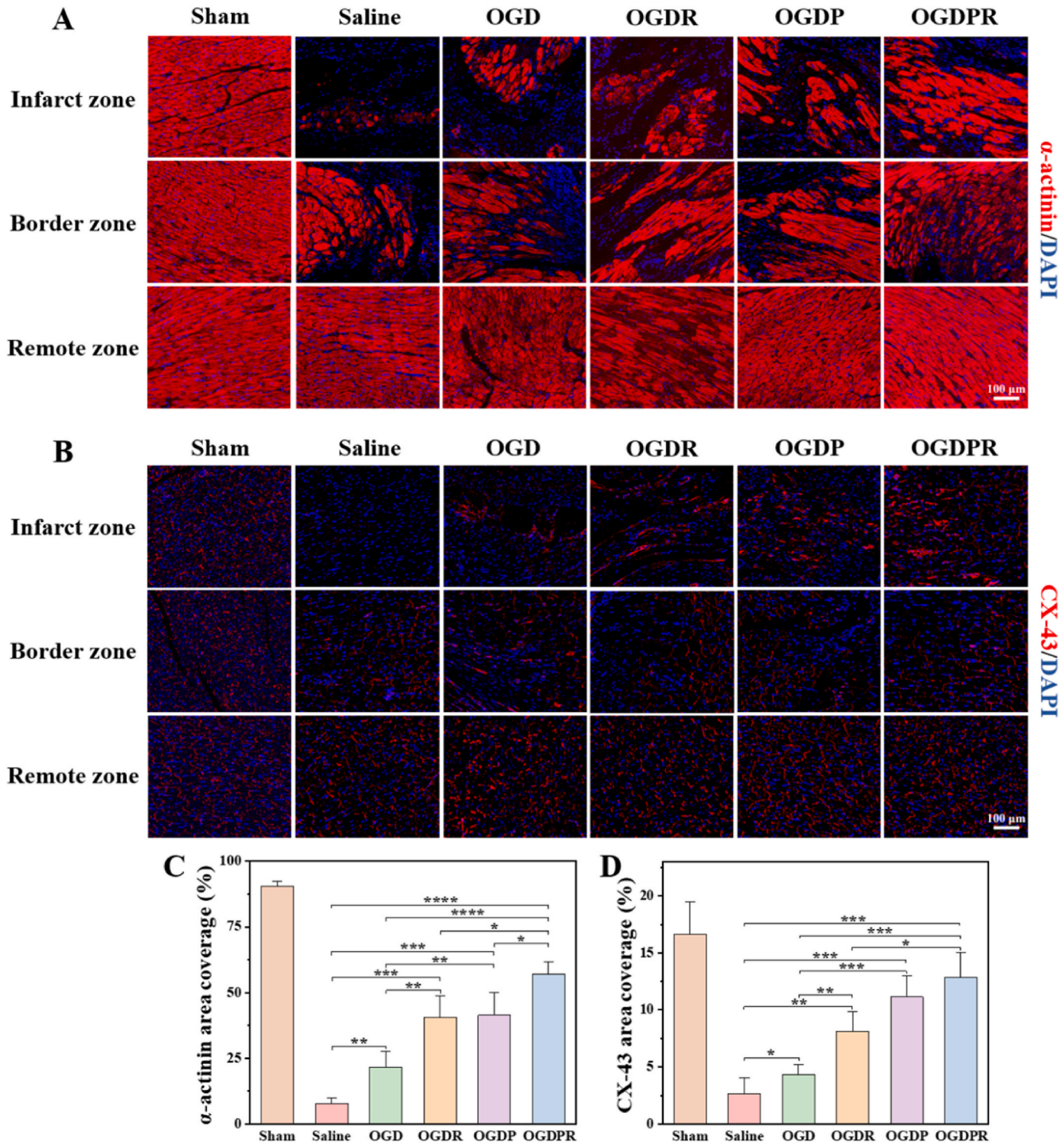

Fig. 10. Hydrogels facilitate the expression of cardiac-specific markers. (A, B) Representative images of α-actinin (A) and CX-43 (B) staining 4 weeks after different treatments. (C, D) Quantitative analysis of α-actinin (C) and CX-43 (D) area coverage in the infarct region (n = 4). *P < 0.05, **P < 0.01, ***P < 0.001, ****P < 0.0001.

Ethics approval and consent to participate

The animal procedures were ratified by the Institutional Animal Care and Use Committee (IACUC) of West China Hospital.

CRediT authorship contribution statement

Linghong Zhang: Conceptualization, Investigation, Methodology, Software, Validation, Formal analysis, Writing – original draft. **Zhongwu Bei:** Investigation, Methodology, Software, Writing – review & editing. **Tao Li:** Investigation, Validation, Formal analysis. **Zhiyong Qian:** Conceptualization, Writing – review & editing, Supervision,

Funding acquisition.

Declaration of competing interest

Zhiyong Qian is an editorial board member for Bioactive Materials and was not involved in the editorial review or the decision to publish this article. All authors declare that there are no competing interests.

Acknowledgments

The authors also greatly appreciate the help of Qing Yang (Research Core Facility, West China Hospital, Sichuan University) for the echocardiographic analysis. This work was financially supported by the National Natural Science Foundation of China (U21A20417), the Sichuan Science and Technology Program (2022YFS0333), the Fundamental Research Funds for the Central Universities (20826041F4138), and 1·3·5 project for disciplines of excellence, West China Hospital, Sichuan University (ZYGD18002).

Appendix A. Supplementary data

Supplementary data to this article can be found online at https://doi.org/10.1016/j.bioactmat.2023.07.007.

References

[1] T. Vos, S.S. Lim, C. Abbafati, K.M. Abbas, M. Abbasi, M. Abbasifard, M. Abbasi-Kangevari, H. Abbastabar, F. Abd-Allah, A. Abdelalim, Global burden of 369 diseases and injuries in 204 countries and territories, 1990–2019: A systematic analysis for the global burden of disease study 2019, The Lancet 396 (10258) (2020) 1204–1222.

[2] M. Zhou, H. Wang, X. Zeng, P. Yin, J. Zhu, W. Chen, X. Li, L. Wang, L. Wang, Y. Liu, J. Liu, M. Zhang, J. Qi, S. Yu, A. Afshin, E. Gakidou, S. Glenn, V.S. Krish, M. K. Miller-Petrie, W.C. Mountjoy-Venning, E.C. Mullany, S.B. Redford, H. Liu, M. Naghavi, S.I. Hay, L. Wang, C.J.L. Murray, X. Liang, Mortality, morbidity, and risk factors in China and its provinces, 1990–2017: a systematic analysis for the global burden of disease study 2017, Lancet 394 (10204) (2019) 1145–1158.

[3] L. Jiao, M. Li, Y. Shao, Y. Zhang, M. Gong, X. Yang, Y. Wang, Z. Tan, L. Sun, L. Xuan, Q. Yu, Y. Li, Y. Gao, H. Liu, H. Xu, X. Li, Y. Zhang, Y. Zhang, LncRNA-*ZFAS1* induces mitochondria-mediated apoptosis by causing cytosolic Ca^{2+} overload in myocardial infarction mice model, Cell Death Dis. 10 (12) (2019) 942.

[4] M.G.S.J. Sutton, N. Sharpe, Left ventricular remodeling after myocardial infarction, Circulation 101 (25) (2000) 2981–2988.

[5] Z. Taimeh, J. Loughran, E.J. Birks, R. Bolli, Vascular endothelial growth factor in heart failure, Nat. Rev. Cardiol. 10 (9) (2013) 519–530.

[6] S.S. Virani, A. Alonso, H.J. Aparicio, E.J. Benjamin, M.S. Bittencourt, C. W. Callaway, A.P. Carson, A.M. Chamberlain, S. Cheng, F.N. Delling, M.S.V. Elkind, K.R. Evenson, J.F. Ferguson, D.K. Gupta, S.S. Khan, B.M. Kissela, K.L. Knutson, C. D. Lee, T.T. Lewis, J. Liu, M.S. Loop, P.L. Lutsey, J. Ma, J. Mackey, S.S. Martin, D. B. Matchar, M.E. Mussolino, S.D. Navaneethan, A.M. Perak, G.A. Roth, Z. Samad, G.M. Satou, E.B. Schroeder, S.H. Shah, C.M. Shay, A. Stokes, L.B. VanWagner, N.-Y. Wang, C.W. Tsao, n. null, Heart disease and stroke statistics—2021 update, Circulation 143 (8) (2021) e254–e743.

[7] J.P. Leach, J.F. Martin, Cardiomyocyte proliferation for therapeutic regeneration, Curr. Cardiol. Rep. 20 (8) (2018) 63.

[8] J. Yu, Biomaterial-based Tissue Engineering Approaches to Repair Myocardial Infarction, University of California, Berkeley with the University of California, San, 2008.

[9] M. Plotkin, S.R. Vaibavi, A.J. Rufaihah, V. Nithya, J. Wang, Y. Shachaf, T. Kofidis, D. Seliktar, The effect of matrix stiffness of injectable hydrogels on the preservation of cardiac function after a heart attack, Biomaterials 35 (5) (2014) 1429–1438.

[10] Y. Matsumura, Y. Zhu, H. Jiang, A. D'Amore, S.K. Luketich, V. Charwat, T. Yoshizumi, H. Sato, B. Yang, T. Uchibori, K.E. Healy, W.R. Wagner, Intramyocardial injection of a fully synthetic hydrogel attenuates left ventricular remodeling post myocardial infarction, Biomaterials 217 (2019), 119289.

[11] J. Zhou, X. Yang, W. Liu, C. Wang, Y. Shen, F. Zhang, H. Zhu, H. Sun, J. Chen, J. Lam, Injectable OPF/graphene oxide hydrogels provide mechanical support and enhance cell electrical signaling after implantation into myocardial infarct, Theranostics 8 (12) (2018) 3317–3330.

[12] T. Yoshizumi, Y. Zhu, H. Jiang, A. D'Amore, H. Sakaguchi, J. Tchao, K. Tobita, W. R. Wagner, Timing effect of intramyocardial hydrogel injection for positively impacting left ventricular remodeling after myocardial infarction, Biomaterials 83 (2016) 182–193.

[13] Z. Zheng, Y. Tan, Y. Li, Y. Liu, G. Yi, C.-Y. Yu, H. Wei, Biotherapeutic-loaded injectable hydrogels as a synergistic strategy to support myocardial repair after myocardial infarction, J. Contr. Release 335 (2021) 216–236.

[14] A.N. Steele, M.J. Paulsen, H. Wang, L.M. Stapleton, H.J. Lucian, A. Eskandari, C. E. Hironaka, J.M. Farry, S.W. Baker, A.D. Thakore, K.J. Jaatinen, Y. Tada, M. J. Hollander, K.M. Williams, A.J. Seymour, K.P. Totherow, A.C. Yu, J.R. Cochran, E.A. Appel, Y.J. Woo, Multi-phase catheter-injectable hydrogel enables dual-stage protein-engineered cytokine release to mitigate adverse left ventricular remodeling following myocardial infarction in a small animal model and a large animal model, Cytokine 127 (2020), 154974.

[15] X. Zhang, Y. Lyu, Y. Liu, R. Yang, B. Liu, J. Li, Z. Xu, Q. Zhang, J. Yang, W. Liu, Artificial apoptotic cells/VEGF-loaded injectable hydrogel united with immunomodification and revascularization functions to reduce cardiac remodeling after myocardial infarction, Nano Today 39 (2021), 101227.

[16] Z. Yuan, Y.-H. Tsou, X.-Q. Zhang, S. Huang, Y. Yang, M. Gao, W. Ho, Q. Zhao, X. Ye, X. Xu, Injectable citrate-based hydrogel as an angiogenic biomaterial improves cardiac repair after myocardial infarction, ACS Appl. Mater. Interfaces 11 (42) (2019) 38429–38439.

[17] J. Zhou, W. Liu, X. Zhao, Y. Xian, W. Wu, X. Zhang, N. Zhao, F.-J. Xu, C. Wang, Natural melanin/alginate hydrogels achieve cardiac repair through ROS scavenging and macrophage polarization, Adv. Sci. 8 (20) (2021), 2100505.

[18] Y. Zhang, Y. Huang, Rational design of smart hydrogels for biomedical applications, Front. Chem. 8 (2021).

[19] W. Yancy Clyde, M. Jessup, B. Bozkurt, J. Butler, E. Casey Donald, M. Colvin Monica, H. Drazner Mark, G. Filippatos, C. Fonarow Gregg, M. Givertz Michael, M. Hollenberg Steven, J. Lindenfeld, A. Masoudi Frederick, E. McBride Patrick, N. Peterson Pamela, W. Stevenson Lynne, C. Westlake, 2016 ACC/AHA/HFSA focused update on new pharmacological therapy for heart failure: an update of the 2013 ACCF/AHA guideline for the management of heart failure, J. Am. Coll. Cardiol. 68 (13) (2016) 1476–1488.

[20] Y. Li, X. Chen, R. Jin, L. Chen, M. Dang, H. Cao, Y. Dong, B. Cai, G. Bai, J. J. Gooding, S. Liu, D. Zou, Z. Zhang, C. Yang, Injectable hydrogel with MSNs/microRNA-21-5p delivery enables both immunomodification and enhanced angiogenesis for myocardial infarction therapy in pigs, Sci. Adv. 7 (9) (2021), eabd6740.

[21] M. Jung, Y. Ma, R.P. Iyer, K.Y. DeLeon-Pennell, A. Yabluchanskiy, M.R. Garrett, M. L. Lindsey, IL-10 improves cardiac remodeling after myocardial infarction by stimulating M2 macrophage polarization and fibroblast activation, Basic Res. Cardiol. 112 (3) (2017) 33.

[22] K. Sun, Y.-y. Li, J. Jin, A double-edged sword of immuno-microenvironment in cardiac homeostasis and injury repair, Signal Transduct. Targeted Ther. 6 (1) (2021) 79.

[23] K. Michaud, C. Basso, G. d'Amati, C. Giordano, I. Kholová, S.D. Preston, S. Rizzo, S. Sabatasso, M.N. Sheppard, A. Vink, A.C. van der Wal, P. on behalf of the Association for European Cardiovascular, Diagnosis of myocardial infarction at autopsy: AECVP reappraisal in the light of the current clinical classification, Virchows Arch. 476 (2) (2020) 179–194.

[24] N. Goonoo, Tunable biomaterials for myocardial tissue regeneration: promising new strategies for advanced biointerface control and improved therapeutic outcomes, Biomater. Sci. 10 (7) (2022) 1626–1646.

[25] J. Zhang, L. Wang, W. Tan, Q. Li, F. Dong, Z. Guo, Preparation of chitosan-rosmarinic acid derivatives with enhanced antioxidant and anti-inflammatory activities, Carbohydr. Polym. 296 (2022), 119943.

[26] M. Nadeem, M. Imran, T. Aslam Gondal, A. Imran, M. Shahbaz, R. Muhammad Amir, M. Wasim Sajid, T. Batool Qaisrani, M. Atif, G. Hussain, B. Salehi, E. Adrian Ostrander, M. Martorell, J. Sharifi-Rad, W.C. Cho, N. Martins, Therapeutic potential of rosmarinic acid: a comprehensive review, Appl. Sci. 9 (15) (2019) 3139.

[27] Y.-Y. Chen, C.-F. Tsai, M.-C. Tsai, W.-K. Chen, Y.-W. Hsu, F.-J. Lu, Anti-fibrotic effect of rosmarinic acid on inhibition of pterygium epithelial cells, Int. J. Ophthalmol. 11 (2) (2018) 189–195.

[28] M. Huerta-Madroñal, J. Caro-León, E. Espinosa-Cano, M.R. Aguilar, B. Vázquez-Lasa, Chitosan – rosmarinic acid conjugates with antioxidant, anti-inflammatory and photoprotective properties, Carbohydr. Polym. 273 (2021), 118619.

[29] Y. Liu, K. Ai, L. Lu, Polydopamine and its derivative materials: Synthesis and promising applications in energy, environmental, and biomedical fields, Chem. Rev. 114 (9) (2014) 5057–5115.

[30] Z. Cui, N.C. Ni, J. Wu, G.-Q. Du, S. He, T.M. Yau, R.D. Weisel, H.-W. Sung, R.-K. Li, Polypyrrole-chitosan conductive biomaterial synchronizes cardiomyocyte contraction and improves myocardial electrical impulse propagation, Theranostics 8 (10) (2018) 2752–2764.

[31] S. He, J. Wu, S.-H. Li, L. Wang, Y. Sun, J. Xie, D. Ramnath, R.D. Weisel, T.M. Yau, H.-W. Sung, R.-K. Li, The conductive function of biopolymer corrects myocardial scar conduction blockage and resynchronizes contraction to prevent heart failure, Biomaterials 258 (2020), 120285.

[32] X. Chen, L. Zhu, X. Wang, J. Xiao, Insight into heart-tailored architectures of hydrogel to restore cardiac functions after myocardial infarction, Mol. Pharm. 20 (1) (2023) 57–81.

[33] J. Xu, C.-W. Wong, S.-h. Hsu, An injectable, electroconductive hydrogel/scaffold for neural repair and motion sensing, Chem. Mater. 32 (24) (2020) 10407–10422.

[34] L. Zhang, T. Li, Y. Yu, K. Shi, Z. Bei, Y. Qian, Z. Qian, An injectable conductive hydrogel restores electrical transmission at myocardial infarct site to preserve cardiac function and enhance repair, Bioact. Mater. 20 (2023) 339–354.

[35] S. Liang, Y. Zhang, H. Wang, Z. Xu, J. Chen, R. Bao, B. Tan, Y. Cui, G. Fan, W. Wang, W. Wang, W. Liu, Paintable and rapidly bondable conductive hydrogels as therapeutic cardiac patches, Adv. Mater. 30 (23) (2018), 1704235.

[36] B. Bhana, R.K. Iyer, W.L.K. Chen, R. Zhao, K.L. Sider, M. Likhitpanichkul, C. A. Simmons, M. Radisic, Influence of substrate stiffness on the phenotype of heart cells, Biotechnol. Bioeng. 105 (6) (2010) 1148–1160.

[37] Z. Zheng, C. Lei, H. Liu, M. Jiang, Z. Zhou, Y. Zhao, C.-Y. Yu, H. Wei, A ROS-responsive liposomal composite hydrogel integrating improved mitochondrial

function and pro-angiogenesis for efficient treatment of myocardial infarction, Adv. Healthcare Mater. 11 (19) (2022), 2200990.
[38] Y. Song, C. Zhang, J. Zhang, N. Sun, K. Huang, H. Li, Z. Wang, K. Huang, L. Wang, An injectable silk sericin hydrogel promotes cardiac functional recovery after ischemic myocardial infarction, Acta Biomater. 41 (2016) 210–223.
[39] Y. He, G. Ye, C. Song, C. Li, W. Xiong, L. Yu, X. Qiu, L. Wang, Mussel-inspired conductive nanofibrous membranes repair myocardial infarction by enhancing cardiac function and revascularization, Theranostics 8 (18) (2018) 5159–5177.
[40] X. Song, X. Wang, J. Zhang, S. Shen, W. Yin, G. Ye, L. Wang, H. Hou, X. Qiu, A tunable self-healing ionic hydrogel with microscopic homogeneous conductivity as a cardiac patch for myocardial infarction repair, Biomaterials 273 (2021), 120811.
[41] C. Song, X. Zhang, L. Wang, F. Wen, K. Xu, W. Xiong, C. Li, B. Li, Q. Wang, M.M. Q. Xing, X. Qiu, An injectable conductive three-dimensional elastic network by tangled surgical-suture spring for heart repair, ACS Nano 13 (12) (2019) 14122–14137.
[42] W. Liu, N. Zhao, Q. Yin, X. Zhao, K. Guo, Y. Xian, S. Li, C. Wang, M. Zhu, Y. Du, F.-J. Xu, C. Wang, J. Zhou, Injectable hydrogels encapsulating dual-functional Au@Pt core–shell nanoparticles regulate infarcted microenvironments and enhance the therapeutic efficacy of stem cells through antioxidant and electrical integration, ACS Nano 17 (3) (2023) 2053–2066.
[43] Y. Yang, D. Lei, S. Huang, Q. Yang, B. Song, Y. Guo, A. Shen, Z. Yuan, S. Li, F.-L. Qing, X. Ye, Z. You, Q. Zhao, Elastic 3D-printed hybrid polymeric scaffold improves cardiac remodeling after myocardial infarction, Adv. Healthcare Mater. 8 (10) (2019), 1900065.
[44] J. Zhan, X. Liao, X. Fan, J. Zhang, H. Li, Y. Cai, X. Qiu, An injectable and conductive TEMPOL/polypyrrole integrated peptide co-assembly hydrogel promotes functional maturation of cardiomyocytes for myocardial infarction repair, Composites, Part B 236 (2022), 109794.
[45] K. Lv, Q. Li, L. Zhang, Y. Wang, Z. Zhong, J. Zhao, X. Lin, J. Wang, K. Zhu, C. Xiao, C. Ke, S. Zhong, X. Wu, J. Chen, H. Yu, W. Zhu, X. Li, B. Wang, R. Tang, J.a. Wang, J. Huang, X. Hu, Incorporation of small extracellular vesicles in sodium alginate hydrogel as a novel therapeutic strategy for myocardial infarction, Theranostics 9 (24) (2019) 7403–7416.
[46] S. Frantz, M. Nahrendorf, Cardiac macrophages and their role in ischaemic heart disease, Cardiovasc. Res. 102 (2) (2014) 240–248.
[47] J. Han, Y.S. Kim, M.-Y. Lim, H.Y. Kim, S. Kong, M. Kang, Y.W. Choo, J.H. Jun, S. Ryu, H.-y. Jeong, J. Park, G.-J. Jeong, J.-C. Lee, G.H. Eom, Y. Ahn, B.-S. Kim, Dual roles of graphene oxide to attenuate inflammation and elicit timely polarization of macrophage phenotypes for cardiac repair, ACS Nano 12 (2) (2018) 1959–1977.
[48] T.F. Lüscher, The sooner, the better: anti-inflammation in acute myocardial infarction, Eur. Heart J. 41 (42) (2020) 4100–4102.
[49] B. Qian, Q. Yang, M. Wang, S. Huang, C. Jiang, H. Shi, Q. Long, M. Zhou, Q. Zhao, X. Ye, Encapsulation of lyophilized platelet-rich fibrin in alginate-hyaluronic acid hydrogel as a novel vascularized substitution for myocardial infarction, Bioact. Mater. 7 (2022) 401–411.
[50] X. Yan, A. Anzai, Y. Katsumata, T. Matsuhashi, K. Ito, J. Endo, T. Yamamoto, A. Takeshima, K. Shinmura, W. Shen, K. Fukuda, M. Sano, Temporal dynamics of cardiac immune cell accumulation following acute myocardial infarction, J. Mol. Cell. Cardiol. 62 (2013) 24–35.
[51] X. Hu, P. Zhang, J. Liu, H. Guan, R. Xie, L. Cai, J. Guo, L. Wang, Y. Tian, X. Qiu, A self-association cross-linked conductive zwitterionic hydrogel as a myocardial patch for restoring cardiac function, Chem. Eng. J. 446 (2022), 136988.
[52] N. Baheiraei, H. Yeganeh, J. Ai, R. Gharibi, M. Azami, F. Faghihi, Synthesis, characterization and antioxidant activity of a novel electroactive and biodegradable polyurethane for cardiac tissue engineering application, Mater Sci Eng C Mater Biol Appl 44 (2014) 24–37.
[53] M. Xie, L. Wang, B. Guo, Z. Wang, Y.E. Chen, P.X. Ma, Ductile electroactive biodegradable hyperbranched polylactide copolymers enhancing myoblast differentiation, Biomaterials 71 (2015) 158–167.
[54] K.C. Michelis, M. Boehm, J.C. Kovacic, New vessel formation in the context of cardiomyocyte regeneration–the role and importance of an adequate perfusing vasculature, Stem Cell Res. 13 (3 Pt B) (2014) 666–682.
[55] S. Park, S. Edwards, S. Hou, R. Boudreau, R. Yee, K.J. Jeong, A multi-interpenetrating network (IPN) hydrogel with gelatin and silk fibroin, Biomater. Sci. 7 (4) (2019) 1276–1280.
[56] W. Xiong, X. Wang, H. Guan, F. Kong, Z. Xiao, Y. Jing, L. Cai, H. Hou, X. Qiu, L. Wang, A vascularized conductive elastic patch for the repair of infarcted myocardium through functional vascular anastomoses and electrical integration, Adv. Funct. Mater. 32 (19) (2022), 2111273.
[57] S. Zhu, C. Yu, N. Liu, M. Zhao, Z. Chen, J. Liu, G. Li, H. Huang, H. Guo, T. Sun, J. Chen, J. Zhuang, P. Zhu, Injectable conductive gelatin methacrylate/oxidized dextran hydrogel encapsulating umbilical cord mesenchymal stem cells for myocardial infarction treatment, Bioact. Mater. 13 (2022) 119–134.
[58] C. Tu, R. Mezynski, J.C. Wu, Improving the engraftment and integration of cell transplantation for cardiac regeneration, Cardiovasc. Res. 116 (3) (2020) 473–475.